Supplementary

Table of Contents

Section 1: Study area and soil sampling

We studied two areas classified as Arctic lowland ice-wedge polygon tundra, located on the coastal plain of the Yukon, Western Canada (Figure 1). The first focus area comprised two small lagoons called Ptarmigan Bay (69°27'N, 139°05'W) and Whale Bay (69°25'N, 138°59'W). The second focus area, approximately 40 km further towards the west, called Komakuk Beach (69°35'N, 140°10'W), is a small coastal catchment positioned between two alluvial fans. Despite their close vicinity, the areas differ in their glaciation history. Throughout the Pleistocene, the areas of Ptarmigan Bay and Whale Bay were covered by ice sheets, whereas the Komakuk Beach further west stayed unglaciated (Dyke and Prest, 1987; Fritz et al., 2012). The surface geology mainly comprises lacustrine, fluvial (Ptarmigan Bay and Komakuk Beach) and morainal deposits (Whale Bay) (Fritz et al., 2012; Rampton, 1982).

The periglacial landscape is characterized by a mosaic of ice-wedge polygon networks, mires, beaded streams, and thermokarst lakes (Rampton, 1982; Speetjens et al., 2022), underlain by continuous permafrost with a high ground ice content (Couture and Pollard, 2017; Westerveld et al., 2023). The climate is classified as Polar Tundra (Beck et al., 2018). Recorded mean annual temperatures (1972 - 2000) at the climate stations Komakuk Beach and Shingle Point (68° 57'N, 137° 13'W) were - 11 °C (± 2.0 °C) and - 9.9 °C (± 4.5 °C). Average summer temperatures (June-August) were 6 °C (± 1.6 °C) and 8.6 °C (± 1.6 °C). Mean annual precipitation (1972 – 2000) was 161 mm and 254 mm correspondingly (Government of Canada, 2024). The vegetation period lasts approximately from June to September (Frank-Fahle et al., 2014). The vegetation map defines the area as bioclimatic subzone E/ low Arctic shrub tundra (Walker et al., 2005).

Differences in microtopography and relief are strong determinants for the identity of the prevailing soil suborder and plant species composition. Turbic Cryosols were present in the drier centres of HCPs and FCPs (Canadian System of Soil Classification, Soil Classification Working Group, 1998). These soils harbor up to 40 cm thick organic horizons with material being of various decomposition stages, followed by a pronounced silt- and clay-rich mineral subsoil layer which commonly exhibits cryoturbations or gleyic features (Tarnocai, 2004). Dwarf-shrubs (e.g., *Betula nana*, *Salix arctica*, *Salix alaxensis*, *Empetrum nigrum*, *Vaccinium sp*.), forbs (e.g., *Rubus chamaemorus, Dryas sp*.) and lichens dominated the centres of HCPs. FCPs were mainly characterised by *Eriophorum vaginatum* tussocks and dwarf-shrubs. Inundated centres of LCP harbored Organic Cryosols, which show a more than 40 cm thick characteristic sequence from fibric to hemic to sapric sphagnum- or sedge- derived material with increasing depth. The dominant plant groups were graminoids (*Carex aquatilis*, *Eriophorum vaginatum, Eriophorum angustifolium*), brown mosses (Amblystegiaceae), and

peat mosses (*Sphagnum sp.*) (Brooks and Lane, 2011; Rampton, 1982; Walker et al., 2005). Towards the drier rims, Organic Cryosols transitioned into Cryosols of the Gleysolic or Static type, indicated by higher dwarf shrub abundance.

Supplementary Table 1(a).: *Sampled soil pits - polygon type, coordinates, and vegetation composition.*

Soil pit	Study Area	Polygon type	N	W	Comments
1	Ptarmigan Bay	HCP	69° 27.862500'	139° 4.939320'	tussock tundra, *Salix sp*., *Betula sp*., *Sphagnum sp*., mosses, lichens
2	Ptarmigan Bay	HCP	69° 27.860040'	139° 5.103600'	*Salix sp*., *Betula sp*., *Empetrum nigrum*, *Dryas sp*., *Vaccinium sp*., lichens
3	Ptarmigan Bay	HCP	69° 27.881220'	139° 5.219760'	*Salix sp*., *Betula sp*., *Rubus chamaemorus*, *Vaccinium sp*., mosses, lichens
4	Whale Bay	FCP	69° 25.561920'	138° 59.929800'	tussock tundra, *Salix sp*., *Betula sp*., graminoids
5	Whale Bay	FCP	69° 25.601040'	139° 0.145080'	tussock tundra, *Salix sp*., Betula sp., *Vaccinium sp*., *Ledum sp.,* mosses
6	Whale Bay	FCP	69° 25.522920'	138° 59.908980'	tussock tundra, *Salix sp*., *Vaccinium sp*., *Ledum sp.,* mosses
7	Ptarmigan Bay	LCP	69° 27.913140'	139° 5.086560'	Sedge-dominated, *Eriophorum sp.*, *Sphagnum sp*., brown mosses
8	Ptarmigan Bay	LCP	69° 27.922800'	139° 5.084160'	Sedge-dominated, *Eriophorum sp*., *Sphagnum sp*., brown mosses
9	Ptarmigan Bay	LCP	69° 27.917880'	139° 5.030940'	Sedge-dominated, *Eriophorum sp*., *Sphagnum sp*., brown mosses
10	Komakuk Beach	HCP	69° 35.590020'	140° 9.880020'	*Betula sp*., *Dryas sp*., *Rubus chamaemorus*, mosses, lichens
11	Komakuk Beach	HCP	69° 35.577000'	140° 9.826980'	*Betula sp*., *Salix sp*., *Vaccinium sp*., *Rubus chamaemorus*, mosses
12	Komakuk Beach	HCP	69° 35.610000'	140° 9.768000'	tussock tundra, *Betula sp*., *Empetrum nigrum*, mosses, lichens, fungi
13	Komakuk Beach	FCP	69° 35.338020'	140° 9.847020'	flat tundra surrounded by wetlands, *Carex sp*., *Salix sp*.
14	Komakuk Beach	FCP	69° 35.551980'	140° 9.454020'	flat tundra, *Carex sp*., *Eriophorum sp., Betula sp*., *Vaccinium sp*., mosses
15	Komakuk Beach	FCP	69° 35.752020'	140° 9.292980'	flat tundra, *Carex sp*., Salix sp., mosses, *Eriophorum sp*.
16	Komakuk Beach	LCP	69° 34.623000'	140° 10.621980'	Sedge-dominated, *Carex sp*., *Salix sp*., *Sphagnum sp*., brown mosses
17	Komakuk Beach	LCP	69° 34.852020'	140° 11.119020'	Sedge-dominated, *Carex sp.*, *Salix sp*., *Sphagnum sp*., brown mosses
18	Komakuk Beach	LCP	69° 34.894980'	140° 10.929000'	Sedge-dominated, *Eriophorum sp*., brown mosses

Dry areas of HCPs were typically dominated by dwarf-shrubs, forbs, and lichen, while in centres of LCPs, the vegetation was adapted to water-saturated conditions and mostly graminoids or peat- and brown-mosses prevailed.

Supplementary Table 1(b): *Sampled soil pits - active layer depths and in-situ soil temperatures.*

Soil pit	Study Area	Polygon type	AL depth (cm)	In-situ Soil Temp (°C)			
				5 cm	15 cm	25 cm	PF Table
1	Ptarmigan Bay	HCP	35.0	7.7	2.5	1.8	1.4
2	Ptarmigan Bay	HCP	30.0	4.5	2.8	1.7	1.5
3	Ptarmigan Bay	HCP	31.0	4.3	3.9	3.6	0.9
4	Whale Bay	FCP	40.0	4.9	1.9	0.9	0.3
5	Whale Bay	FCP	40.0	4.4	4.0	2.5	1.9
6	Whale Bay	FCP	40.0	7.7	2.9	2.3	1.2
7	Ptarmigan Bay	LCP	40.0	4.8	4.4	3.8	2.0
8	Ptarmigan Bay	LCP	30.0	3.8	3.6	3.4	2.5
9	Ptarmigan Bay	LCP	30.0	6.6	5.6	4.5	n.a.
10	Komakuk Beach	HCP	30.0	5.1	3.4	2.4	1.6
11	Komakuk Beach	HCP	22.5	3.6	2.5	-	1.5
12	Komakuk Beach	HCP	30.5	5.5	4.5	3.6	2.3
13	Komakuk Beach	FCP	28.0	7.4	2.5	1.4	0.4
14	Komakuk Beach	FCP	30.0	4.7	4.3	3.4	2.6
15	Komakuk Beach	FCP	22.5	4.6	1.1	-	0.1
16	Komakuk Beach	LCP	45.0	6.6	6.2	4.7	0.8
17	Komakuk Beach	LCP	52.0	6.8	5.6	3.6	n.a.
18	Komakuk Beach	LCP	40.0	5.7	4.3	3.0	0.2

Average active layer depth was ~ 30 cm in HCPs, ~33 cm in FCPs, and ~40 cm in LCPs. Average in-situ soil temperatures declined from 5.5 ± 0.3 °C (mean ± stderr) at the surface (5 cm depth), to 3.7 ± 0.3 °C at 15 cm depth, to 2.9 ± 0.3 °C in 25 cm depth to 1.3 ± 0.2 °C at the permafrost table, respectively.

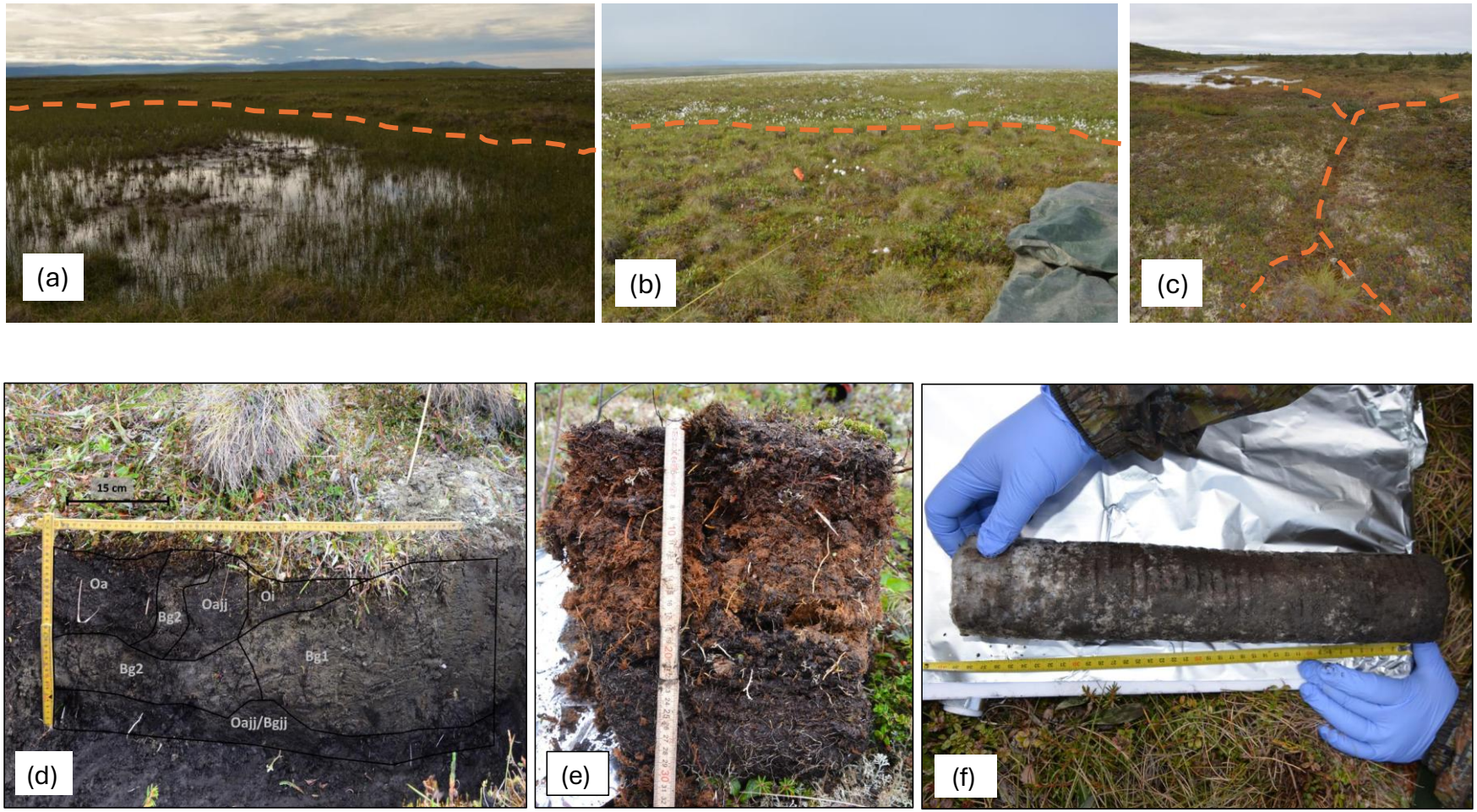

Supplementary Figure 1: *Examples for investigated ice-wedge polygon types and soil layers. Orange dotted lines roughly mark polygon borders. (a) Low-centered polygon (LCP), with dry, elevated rim around inundated center; (b) Flat-centered polygon (FCP) with presence of cotton grass indicating wetter trough*

around flat-center;, (c) High-centered polygon (HCP), with presence of mosses indicating wetter troughs around drier, elevated centres; (d) active layer sampling from soil pits (applied for HCPs and FCPs). Horizon boundaries (perspective corrected) were drawn on the image:(Source: Wagner et al., 2023).(e) active layer sampling from LCPs (extracted peat block). (f) frozen permafrost sampling (example for core that was extracted via gas powered SIPRE corer; note that 'permafrost layer' in this manuscript refers to the upper 10 cm, respectively). Photo credits: Julia Wagner and Victoria Martin.

Section 2: Physicochemical soil parameters and stoichiometry

In the field, samples were weighed for bulk density measurements (see Wagner et al., 2023). Gravimetric soil water content (g H_2O g^{-1} DW) was determined at the facilities of the Aurora Research Institute, Inuvik, Canada, before transporting the samples to Vienna (80 °C for 48 hours). Soil pH was determined in a 1:5 (w/v) soil:MQ water slurry using a Sentron SI600. Aliquots of dry soils were ground to fine powder using a ball-mill (MM-2000, Retsch, Germany). Subsequently, 1-8 mg per sample (depending on the anticipated differences in C content between soil layer categories) were weighed into tin capsules and analyzed for total carbon (mg C g^{-1} DW) and nitrogen (mg N g^{-1} DW) contents via elemental analyzer (EA 1110, CE Instruments, Italy) coupled to a continuous-flow isotopic ratio mass spectrometer (IRMS, DeltaPlus, Finnigan MAT). The soils did not contain any carbonates, which was tested by adding 1M HCl to the samples before subjecting them to the EA-IRMS. Isotopic signatures ($\delta^{13}C$, $\delta^{15}N$, ‰) were expressed relative to the international standard VPDB. Soil C:N, C:P, and N:P ratios were calculated on a mass basis. Pools of dissolved C and N (DOC, TDN; mg g^{-1} DW) were determined with a TOC/TN-Analyzer (Shimadzu TOC-VCP/CPNTNM-1, Shimadzu, Korneuburg, Austria) in 1M KCl extracts (soil to solution ratio 1:7.5 (w/v)). The soil total phosphorus pool (Soil P) was obtained via a modified ignition method by Kuo (1996), which mediates the conversion of organic bound P to inorganic P. Therefore, 200 - 500 mg dry and milled soils were combusted for 5 h at 450 °C, (muffle device Heraeus M1100/1) and then extracted for 16 hours with 10 ml 0.5M H_2SO_4. Soil total Phosphorus concentrations (mg P g^{-1} DW) were measured in the fresh extracts following the photometric malachite-green assay after D'Angelo and Crutchfield, 2001. All above mentioned extracts have been filtered using Whatman™ quantitative ashless cellulose filter paper, grade 40.

Supplementary Table 2(a).: *Physicochemical soil parameters and stoichiometry across ice-wedge polygon types.*

	LCP	FCP	HCP	Polygon Type Effect
pH (MQ)	5.72 ± 0.09 (b)	5.92 ± 0.05 (a)	5.66 ± 0.06 (b)	**p = 4.3 e^{-3}** (Chi^2 = 10.92)
SWC (g g^{-1} DW)	2.93 ± 0.33 (a)	2.20 ± 0.32 (a)	2.03 ± 0.27 (a)	p = 0.603 (F = 0.51)
δ^{13}C (‰)	-27.90 ± 0.13 (a)	-26.73 ± 0.12 (b)	-27.42 ± 0.18 (a)	**p = 1.6 e^{-5}** (Chi^2 = 22.1)
δ^{15}N (‰)	0.34 ± 0.13 (b)	1.31 ± 0.20 (a)	1.63 ± 0.22 (a)	**p = 2.3 e^{-3}** (F = 9.77)
Soil C (mg g^{-1} DW)	312.37 ± 30.81 (a)	204.19 ± 21.68 (a)	229.65 ± 23.34 (a)	**p = 0.059** (F = 3.31)
Soil N (mg g^{-1} DW)	18.1 ± 1.90 (a)	10.04 ± 0.91 (b)	12.14 ± 1.21 (b)	**p = 2.8 e^{-3}** (Chi^2 = 11.72)
Soil P (mg g^{-1} DW)	0.43 ± 0.03 (*int)	0.68 ± 0.05 (*int) [n=30]	0.63 ± 0.06 (*int)	**p = 7.0 e^{-3}** (F = 5.34)
Soil C:N	17.54 ± 0.37 (a)	20.09 ± 1.57 (a)	19.42 ± 0.98 (a)	p = 0.375 (Chi^2 = 3.11)
Soil C:P	783.09 ± 91.44 (a)	305.98 ± 31.02 (b) [n=30]	389.45 ± 37.03 (b)	**p = 4.8 e^{-5}** (F = 22.07)
Soil N:P	45.06 ± 5.30 (a)	15.49 ± 1.04 (b) [n=30]	20.05 ± 1.70 (b)	**p = 8.8 e^{-6}** (F = 37.7)
DOC (µg g^{-1} DW)	551.99 ± 76.89 (a)	355.06 ± 64.63 (a)	400.95 ± 87.34 (a)	p = 0.076 (Chi^2 = 5.15)
TDN (µg g^{-1} DW)	38.51 ± 6.07 (a)	26.63 ± 7.57 (a)	30.89 ± 6.14 (a)	p = 0.404 (F = 0.95)
DOC:TDN	17.69 ± 2.66 (a)	20.49 ± 3.21 (a)	16.01 ± 2.32 (a)	p = 0.122 (F = 2.17)

*Presented are means ± standard error (n_LCP=20, n_FPT=32, n_HCP=29; with individual deviations noted in the table). Statistical results from linear mixed-effects models (Type II ANOVA p-values and F-statistics) are shown in the right column. When model assumptions were not met, Kruskal Wallis tests were used (p-values and Chi² statistics). Pairwise comparisons (Tukey-adjusted emmeans or Bonferroni-adjusted pairwise Wilcoxon tests) are indicated by letter groupings in brackets. Significant interactions between polygon type and soil layer are marked with (*int).*

Interactive effects:

Soil P (mg g-1 DW) was significantly lower in the organic layer of LCPs compared to FCPs and HCPs (lme: p=0.049, F=2.4; emmeans pairwise test_organic: LCP vs. FCP p=0.0001, t=-4.5; LCP vs. HCP p<0.0001, t=-4.8). Abbreviations: SWC= soil water content, DOC= dissolved organic C, TDN= total dissolved N.

***Supplementary Table 2(b)**.: Physicochemical soil parameters and stoichiometry across soil layer categories*.

	organic	mineral	cryoturbated	permafrost	Soil Layer Effect
pH (MQ)	5.63 ± 0.06 (b)	5.91 ± 0.06 (ab)	5.80 ± 0.09 (ab)	5.94 ± 0.06 (a)	**p = 9.3 e^{-3}** (Chi^2 = 11.51)
SWC (g g^{-1} DW)	3.72 ± 0.23 (a)	0.45 ± 0.03 (c)	1.41 ± 0.19 (b)	1.75 ± 0.18 (b)	**p = 2.0 e^{-16}** (F = 80.21)
δ^{13}C (‰)	-27.34 ± 0.15 (a)	-27.59 ± 0.26 (a)	-27.16 ± 0.23 (a)	-26.96 ± 0.17 (a)	p = 0.203 (Chi^2 = 4.60)
δ^{15}N (‰)	1.39 ± 0.20 (a)	1.58 ± 0.29 (ab)	1.04 ± 0.21 (bc)	0.61 ± 0.26 (c)	**p = 1.2 e^{-4}** (F= 8.14)
Soil C (mg g^{-1} DW)	351.19 ± 15.53 (a)	63.33 ± 7.58 (c)	185.39 ± 19.29 (b)	202.80 ± 19.33 (b)	**p = 2.0 e^{-16}** (F = 63.24)
Soil N (mg g^{-1} DW)	18.42 ± 1.03 (a)	3.65 ± 0.40 (c)	10.11 ± 1.09 (b)	10.95 ± 0.89 (b)	**p = 7.5 e^{-11}** (Chi^2 = 50.12)
Soil P (mg g^{-1} DW)	0.73 ± 0.05 (*int) [n=34]	0.46 ± 0.05 (*int) [n=13]	0.54 ± 0.07 (*int)	0.49 ± 0.04 (*int)	**p = 6.1 e^{-6}** (F = 10.92)
Soil C:N	20.69 ± 1.57 (a)	17.41 ± 0.91 (a)	18.64 ± 0.59 (a)	18.24 ± 0.44 (a)	p = 0.375 (Chi^2 = 3.11)
Soil C:P	590.98 ± 64.14 (a) [n=34]	158.62 ± 16.14 (b) [n=13]	374.08 ± 38.28 (a)	479.85 ± 62.08 (a)	**p = 4.9 e^{-10}** (F = 23.11)
Soil N:P	31.67 ± 3.73 (a) [n=34]	8.80 ± 0.70 (b) [n=13]	20.07 ± 1.92 (a)	26.06 ± 3.37 (a)	**p = 2.1 e^{-11}** (F = 28.66)
DOC (µg g^{-1} DW)	739.61 ± 68.61 (a)	59.74 ± 5.07 (c)	173.95 ± 25.55 (b)	265.52 ± 46.41 (b)	**p = 1.0 e^{-11}** (Chi^2 = 54.21)
TDN (µg g^{-1} DW)	50.36 ± 7.52 (a)	4.04 ± 0.74 (c)	15.54 ± 2.63 (b)	26.16 ± 4.82 (b)	**p = 1.2 e^{-15}** (F = 44.92)
DOC:TDN	22.13 ± 3.19 (a)	22.16 ± 3.83 (a)	13.19 ± 1.69 (b)	11.43 ± 1.07 (b)	**p = 9.4 e^{-5}** (F = 8.22)

*Presented are means ± standard error (n_organic=35; n_mineral=14; n_cryoturbated=13, n_permafrost=19; with individual deviations noted in the table). Statistical results from linear mixed-effects models (Type II ANOVA p-values and F-statistics) are shown in the right column. When model assumptions were not met, Kruskal Wallis tests were used (p-values and Chi² statistics). Pairwise comparisons (Tukey-adjusted emmeans or Bonferroni-adjusted pairwise Wilcoxon tests) are indicated by letter groupings in brackets. Significant interactions between polygon type and soil layer are marked with (*int).*

***Interactive effects:** In LCPs, soil layers had similar soil P concentrations, while in FCPs and HCPs, the organic layer had higher P concentrations compared to the mineral and permafrost layers (lme: p=0.049, F=2.4; emmeans pairwise test_organic vs.mineral: FCP: p=0.0002, t=4.6; HCP: p=0.0017, t=3.9; organic vs. permafrost: FCP: p=0.063, t=2.6; HCP: p=0.005, t=3.5). Abbreviations: SWC= soil water content, DOC= dissolved organic C, TDN= total dissolved N).*

1

Section 3: Chemical composition of soil organic matter

We used Pyrolysis- GC/MS for obtaining characteristic fingerprints of the chemical composition of the soil organic matter pools among the investigated ice-wedge polygon types and soil layer categories. Therefore, we used a semi-automated approach as explained in (Martin et al., 2024), with minor adaptations.

Approximately 0.1 to 0.2 mg of dried and finely milled soil samples were weighed into pyrolysis glass tubes (constricted Quartz Tubes for 6000 DISC and Autosampler, CDS Analytical) deploying a randomized sample order. Ideal sample amounts (adapted to respective soil C concentrations) were determined in pre-tests. We compiled a mixed reference sample out of four randomly selected samples, representing different soil layers, polygon types and sampling areas. To ensure consistent quality of the instruments' performance throughout the runs we included multiple technical replicates of an external soil standard (IHSS Elliott Soil Humic Acid Standard IV) as well as for the mixed reference sample. To account for possible contamination of the glass tubes, we included several blanks throughout the sample sequence. Samples were pyrolyzed (Pyroprobe 6200 and Autosampler 6250T, CDS) at an initial temperature of 50 °C (5 sec) followed by a ramp increase of 20 °C/sec and a final temperature of 600 °C (20 sec). Pyrolysis products were transferred into the GC-TOF-MS system (Pegasus BT GC-MS, LECO) with a constant target flow of 1mL helium/min at 280 °C. After each sample the pyrolysis chamber was heated to 1,000 °C for 60 seconds and flushed clean for the next sample. A polar column (Supelcowax TM 10 Fused Silica Capillary Column, 30 m x 0.25 mm x 0.25 µm film thickness, Sigma- Aldrich) was used. The GC was kept at 50 °C (2 min), followed by an increase of 7 °C/min until reaching the final temperature of 250 °C (5 min). All resulting chromatograms were analyzed with ChromaTOF software (version 5.51.50.068774, LECO).

After visually checking the regularity of the chromatograms from the three technical replicates of the mixed reference sample, one was selected for subsequent manual analysis and creation of a so-called "reference sample compound library". Therefore, we compared the mass spectrum of each individual peak within the chromatogram to suggested spectra from the electron ionization (EI) mass spectral libraries "mainlib" and "replib", contained in the NIST Library of Mass Spectrometry (U.S. Department of Commerce National Institute of Standards and Technology). Prior to confirming the identity of an individual substance, we additionally consulted (i) the fit to in literature reported retention times, (ii) revised the substances' relative position within a sequence of other identified compounds (this is particularly helpful for long-chained alkanes) and (iii) compared the in ChromaTOF included probability assessment of the observed ion m/z versus expected ion m/z. Following this process, we obtained a list of

identified (e.g., “1-Dodecene”) compounds plus compounds which we could not clearly assign to an entry from the NIST libraries, but which we could identify via their unique mass spectrum (e.g., “Peak_1”).

From this data, we created a library of pyrolysis products that was employed for the subsequent semi-automated analysis of all samples and blanks. Hence, only substances that were included in the library were considered for the subsequent steps. Since this library of pyrolysis products is project specific, it holds representative characteristics of the SOM pool of the respective sampling area. We employed the library-matching algorithm implemented in ChromaTOF and performed an automated targeted compound search for all compounds contained in the library. In this manner, we could reference substances within samples and blanks to those of the library. The m/z spectrum of every peak within an extracted- ion sample chromatogram (XIC) was compared to the deconvoluted spectrum of the substance from the library. A similarity match score (min. score = 1, max. score= 1000) provided information about the respective fit of the match. For the process of automated hit assignment, we set the minimum similarity match threshold to > 700 (the reliability of this threshold was evaluated during pre-tests in the phase of method development). Further, we set the threshold of the min. peak signal to noise ratio (S/N) >100 to remove background noise within the chromatograms. After completion of the automated assignments via the algorithm, we manually checked the correctness of the automatically matched pyrolysis substances (e.g., “1-Dodecene”, “Peak_1”) by visual assessment and corrected wrong assignments. Such manual confirmation avoids wrong assignments due to very similar spectra (such as i.e., found with long-chained alkanes), but also allows to include the small fraction of compounds into the dataset, where manual identification is possible, but where the automatic matching algorithm failed (due to not meeting the similarity-threshold-criterium). Following these steps, we derived a presence-absence list from all pyrolysis products listed in the library (“1-Dodecene”, “Peak_1”), plus their corresponding peak areas from all soil samples and blanks. To control for possible contamination in the pyrolysis system or the glass tubes, a blank correction step was performed on the dataset. Therefore, we subtracted mean areas of substances found in blanks from the area of the respective substance within the samples. Further, we normalized the sample chromatogram peak areas with respective soil carbon contents and the pyrolyzed amount of sample, as both factors can influence peak area and baseline height. Following the assumption that the sum of all pyrolysis-product-areas within a sample equals its carbon content, allowed us to calculate individual substance abundances (mg C g^{-1} soil DW).

We employed the phyloseq” package (McMurdie and Holmes, 2013) for handling the dataset, with (i) substance abundances being equivalent to the OTU-abundance matrix, (ii) SOM compound group classification being equivalent to taxonomic information, and (iii) metadata

including information on polygon type and soil layer category. We excluded rare pyrolysis compounds accounting for less than 0.1 % of the total C content per sample. This step helped to reduce the size of the dataset by identifying those substances with a significant contribution to the respective overall sample peak area. From a total of 1387 pyrolysis products in the initial dataset, 534 were consequentially considered for the final SOM fingerprint.

We assigned these 534 pyrolysis products to the following SOM compound groups: (1) “aromatics & phenols [n=51]”, (2) “carbohydrates” [n=48], (3) “N-containing compounds” [n=42], (4) “lignin-derived compounds” [n=16], and (5) “lipids” [n=68], with the classification being supported by literature (Buurman et al., 2005; González-Pérez et al., 2012; Hempfling and Schulten, 1990; Ninnes et al., 2017; Said et al., 2015; Saiz-Jimenez and De Leeuw, 1986; Schulten and Schnitzer, 1997; Shen et al., 2018; Stewart, 2012; Tolu et al., 2015; Vancampenhout et al., 2009). In case of no available literature reference, we assigned the compound to one of the mentioned SOM groups based on their molecular structure, employing the US National Library of Medicine (NCBI) PubChem compound database (Kim et al., 2023). We summarized substances that we could not assign to one of the aforementioned compound groups (e.g., “Cyclononasiloxane“), plus all compounds that were matched to a nameless substance in the library (e.g., “Peak_1”) in a group that we called (6) “general & unknown compounds” [n=309].

92 ***Supplementary Table 3.:*** *Assignment of pyrolysis products into SOM compound groups.*

Aromatics & Phenols	
1-Butanone, 1-(2-furanyl)-	3-Methylphenylacetylene
1H-Inden-1-one, 2,3-dihydro-	9H-Fluorene, 9-methylene-
1H-Indene, 1,1-dimethyl-	Acetophenone, 4-hydroxy-
1H-Indene, 1-ethylidene-	Azulene
1H-Indene, 1-methyl-	Benzene, (1,3-dimethylbutyl)-
1-Naphthalenol	Benzene, (2-methyl-1-propenyl)-
2,4-Di-tert-butylphenol	Benzene, (2-methylpropyl)-
2-Methylindene	Benzene, 1-ethyl-2-methyl-
2-Naphthalenol	Benzene, 1-ethyl-3-methyl-
Benzene, 1-methoxy-4-methyl-	Mesitylene
Benzene, 1-methyl-4-(1-methylethenyl)-	Naphthalene
Benzene, 1-methyl-4-propyl-	Naphthalene, 1,7-dimethyl-
Benzene, 1-propenyl-	o-Xylene
Benzene, 2-propenyl-	p-Cresol
Benzene, heptyl-	Phenol
Benzene, hexyl-	Phenol, 2,3-dimethyl-
Benzene, octyl-	Phenol, 2,6-dimethyl-
Benzene, pentyl-	Phenol, 2-ethyl-
Benzene, propyl-	Phenol, 2-methyl-
Benzene, tetradecyl-	Phenol, 3-methyl-
Ethanone, 1-(3-hydroxyphenyl)-	Phenol, 4-ethyl-
Ethylbenzene	Phenol, 4-ethyl-2-methyl-
Fluorene	Phenol, 4-ethyl-3-methyl-
Hydroquinone	p-Xylene
Indane	Styrene

Carbohydrates	
2-Nonadecanone	2-Heptadecanone
1,2-Cyclopentanedione, 3-methyl-	2H-Pyran-2-one, 5,6-dihydro-
1,4:3,6-Dianhydro-a-d-glucopyranose	2-Nonanone
1-Penten-3-one	2-Pentadecanone
2(3H)-Furanone, 5-acetyldihydro-	2-Propanone, 1-(acetyloxy)-
2(3H)-Furanone, 5-methyl-	2-Tridecanone

2(3H)-Furanone, dihydro-3-methylene-	2-Undecanone
2(5H)-Furanone, 5-methyl-	2-Vinylfuran
2,3-Pentanedione	3-Buten-2-one, 3-methyl-
2,4(3H,5H)-Furandione, 3-ethyl-	3-Furaldehyde
2,5-Furandicarboxaldehyde	3-Penten-2-one
2-Cyclopenten-1-one	4-Cyclopentene-1,3-dione
2-Cyclopenten-1-one, 2,3-dimethyl-	5-Hydroxymethylfurfural
2-Cyclopenten-1-one, 2-methyl-	6H-Dibenzo[b,d]-pyran
2-Cyclopenten-1-one, 3-methyl-	Benzofuran
2-Furancarboxaldehyde, 5-methyl-	Benzofuran, 2,3-dihydro-
Benzofuran, 2-methyl-	Furan, 2-ethyl-
Cyclobutanone, 2,2-dimethyl-	Furan, 2-methyl-
Cyclohexanone	Furan, 2-propyl-
Cyclopentanone	Furan, 3-methyl-
Dibenzofuran	Furaneol
Dihydro-2(3H)-thiophenone	Furfural
Ethanone, 1-(2-furanyl)-	Levoglucosenone
Furan, 2,5-dimethyl-	Maleic anhydride
Lignins & Lignin-derived compounds	
2-Methoxy-4-vinylphenol	Ethanone, 1-(4-hydroxy-3,5-dimethoxyphenyl)-
3-Methoxy-5-methylphenol	Phenol, 2,6-dimethoxy-
Apocynin	Phenol, 2,6-dimethoxy-4-(2-propenyl)-
Benzaldehyde	Phenol, 2-methoxy-
Benzaldehyde, 3-hydroxy-	Phenol, 2-methoxy-4-(1-propenyl)-
Benzaldehyde, 4-hydroxy-	Phenol, 4-ethenyl-2,6-dimethoxy-
Benzaldehyde, 4-hydroxy-3,5-dimethoxy-	Phenol, 4-ethyl-2-methoxy-
Creosol	Vanillin
Lipids	
1,2-Nonadiene	1-Pentadecene
1,3,5-Cycloheptatriene	1-Tetradecene
1,3,8-p-Menthatriene	1-Tricosene
10-Heneicosene (c,t)	1-Tridecene
1-Docosene	1-Undecene
1-Dodecanol, 2-octyl-	2,4-Dimethyl-1-heptene

1-Dodecene	2,6,10-Trimethyltridecane
1-Heptacosanol	2-Butanone, 1-(acetyloxy)-
1-Heptadecene	2-Butenal, (E)-
1-Hexacosanol	2-Propenal
1-Hexacosene	2-Tridecene, (E)-
1-Hexadecanol	3-Eicosene, (E)-
1-Hexadecene	3-Methyl-2-furoic acid
1-Hexanol	cis-13-Eicosenoic acid
1-Nonadecene	Cycloeicosane
1-Nonene	Cyclohexadecane
1-Octadecene	Cyclohexene
Cyclopropane, 1,2-dimethyl-, trans-	n-Hexadecanoic acid
Cyclotetracosane	Nonadecane
Decane	Nonane
Docosane	Octacosanol
Docosanoic acid, methyl ester	Octadecane
Dodecanal	Octane
Dodecane	Pentacosane
Dodecane, 2,6,10-trimethyl-	Pentadecane
Eicosane	Propanoic acid, 2-hydroxy-2-methyl-, methyl ester
Erucic acid	Propanoic acid, anhydride
Heneicosane	Tetradecane
Heptacosane	Tetradecanoic acid
Heptadecane	Tricosane
Hexacosane	Tridecane
Hexadecane	Tridecane, 7-methylene-
Hexanedioic acid, dioctyl ester	Undecane
Neophytadiene	Undecane, 3-methyl-

N-containing substances

1H-Imidazole	4-Pyridinone
1H-Pyrrole, 1-ethyl-	Acetamide, N-4-pyridinyl-
1H-Pyrrole, 1-methyl-	Benzenepropanenitrile
1H-Pyrrole, 2,4-dimethyl-	Benzonitrile
1H-Pyrrole, 2,5-dimethyl-	Benzonitrile, 3-methyl-

1H-Pyrrole, 2-methyl-	Benzyl nitrile
1H-Pyrrole, 3-methyl-	Difluoramine
1H-Pyrrole-2-carboxaldehyde	Ethyl isocyanide
1H-Pyrrole-3-carbonitrile	Formic acid hydrazide
2(1H)-Pyridinone, 3-methyl-	Hydrazine, 1,1-dipropyl-
2,3-Pyridinedicarbonitrile	Hydrazine, trimethyl-
2,5-Pyrrolidinedione, 1-methyl-	Indole
2-Amino-4-methylpyrimidine	Indole, 3-methyl-
2H-Indol-2-one, 1,3-dihydro-	Phenol, 4-amino-
2-Naphthalenamine	Propanenitrile
4-Aminopyrimidine	Pyridine
Pyridine, 2,3-dimethyl-	Pyridine, 4-methyl-
Pyridine, 2,5-dimethyl-	Pyrrole
Pyridine, 2-methyl-	s-Triazole, 3-acetamido-
Pyridine, 3-methoxy-	Succinimide
Pyridine, 3-methyl-	Urea, methyl-

Compounds of General & Unknown Origin

Cyclononasiloxane, octadecamethyl-

Peak_3	Peak_72
Peak_4	Peak_77
Peak_6	Peak_81
Peak_8	Peak_85
Peak_11	Peak_87
Peak_13	Peak_91
Peak_17	Peak_95
Peak_19	Peak_97
Peak_22	Peak_101
Peak_23	Peak_111
Peak_25	Peak_112
Peak_26	Peak_115
Peak_29	Peak_122
Peak_30	Peak_127
Peak_33	Peak_131
Peak_34	Peak_138

Peak_35
Peak_36
Peak_37
Peak_42
Peak_45
Peak_46
Peak_51
Peak_55
Peak_58
Peak_61
Peak_64
Peak_210
Peak_215
Peak_221
Peak_238
Peak_243
Peak_261
Peak_275
Peak_277
Peak_283
Peak_286
Peak_287
Peak_299
Peak_306
Peak_310
Peak_315
Peak_320
Peak_321
Peak_335
Peak_345
Peak_350
Peak_358
Peak_366
Peak_368
Peak_382
Peak_145
Peak_153
Peak_158
Peak_160
Peak_161
Peak_173
Peak_184
Peak_186
Peak_190
Peak_196
Peak_200
Peak_469
Peak_471
Peak_476
Peak_477
Peak_479
Peak_481
Peak_490
Peak_498
Peak_500
Peak_508
Peak_540
Peak_542
Peak_562
Peak_565
Peak_566
Peak_571
Peak_573
Peak_574
Peak_589
Peak_591
Peak_594
Peak_595
Peak_599
Peak_620

Peak_409
Peak_413
Peak_425
Peak_427
Peak_430
Peak_437
Peak_446
Peak_447
Peak_448
Peak_467
Peak_468
Peak_683
Peak_696
Peak_711
Peak_727
Peak_731
Peak_738
Peak_741
Peak_745
Peak_748
Peak_760
Peak_771
Peak_785
Peak_786
Peak_787
Peak_800
Peak_803
Peak_807
Peak_808
Peak_820
Peak_822
Peak_825
Peak_834
Peak_837
Peak_839
Peak_627
Peak_635
Peak_641
Peak_642
Peak_643
Peak_651
Peak_668
Peak_672
Peak_676
Peak_677
Peak_682
Peak_929
Peak_931
Peak_934
Peak_938
Peak_952
Peak_953
Peak_959
Peak_978
Peak_988
Peak_991
Peak_997
Peak_998
Peak_1007
Peak_1013
Peak_1024
Peak_1036
Peak_1039
Peak_1057
Peak_1059
Peak_1075
Peak_1088
Peak_1092
Peak_1095
Peak_1121

Peak_840
Peak_841
Peak_846
Peak_849
Peak_858
Peak_874
Peak_880
Peak_883
Peak_887
Peak_915
Peak_916
Peak_1175
Peak_1193
Peak_1194
Peak_1198
Peak_1199
Peak_1207
Peak_1214
Peak_1217
Peak_1226
Peak_1231
Peak_1232
Peak_1235
Peak_1237
Peak_1241
Peak_1245
Peak_1246
Peak_1253
Peak_1265
Peak_1274
Peak_1279
Peak_1283
Peak_1286
Peak_1288
Peak_1290
Peak_1125
Peak_1139
Peak_1141
Peak_1144
Peak_1151
Peak_1155
Peak_1157
Peak_1159
Peak_1165
Peak_1166
Peak_1171
Peak_1348
Peak_1349
Peak_1355
Peak_1357
Peak_1383
Peak_1406
Peak_1408
Peak_1417
Peak_1419
Peak_1422
Peak_1424
Peak_1438
Peak_1444
Peak_1450
Peak_1462
Peak_1466
Peak_1467
Peak_1468
Peak_1470
Peak_1472
Peak_1479
Peak_1481
Peak_1485
Peak_1488

Peak_1292	Peak_1492
Peak_1293	Peak_1497
Peak_1294	Peak_1500
Peak_1301	Peak_1503
Peak_1305	Peak_1508
Peak_1310	Peak_1509
Peak_1314	Peak_1522
Peak_1317	Peak_1525
Peak_1323	Peak_1529
Peak_1332	Peak_1531
Peak_1336	Peak_1532
Peak_1548	Peak_1678
Peak_1549	Peak_1679
Peak_1552	Peak_1684
Peak_1563	Peak_1685
Peak_1566	Peak_1691
Peak_1571	Peak_1696
Peak_1579	Peak_1709
Peak_1584	Peak_1716
Peak_1586	Peak_1717
Peak_1589	Peak_1720
Peak_1599	Peak_1723
Peak_1600	Peak_1724
Peak_1607	Peak_1726
Peak_1608	Peak_1742
Peak_1614	Peak_1743
Peak_1638	Peak_1751
Peak_1645	Peak_1754
Peak_1651	Peak_1760
Peak_1657	Peak_1762
Peak_1663	Peak_1764
Peak_1664	Peak_1766
Peak_1665	Peak_1768

93

Supplementary Table 4.: *Correlations between SOM compound groups abundances and soil C content.*

Compound Class (mg C g^{-1} DW)	Soil C (mg g^{-1} DW)
Aromatics & Phenols	ρ (79) = 0.92; **p = < 2.2 e^{-16}**
Carbohydrates	ρ (79) = 0.95; **p = < 2.2 e^{-16}**
General & Unknown	ρ (79) = 0.92; **p = < 2.2 e^{-16}**
Lignins	ρ (79) = 0.77; **p = < 2.2 e^{-16}**
Lipids	ρ (79) = 0.90; **p = < 2.2 e^{-16}**
N- Containing	ρ (79) = 0.98; **p = < 2.2 e^{-16}**

Presented are the Spearman's rank-order correlation coefficient rho (ρ(df)) and respective p-values (two-sided test).

94

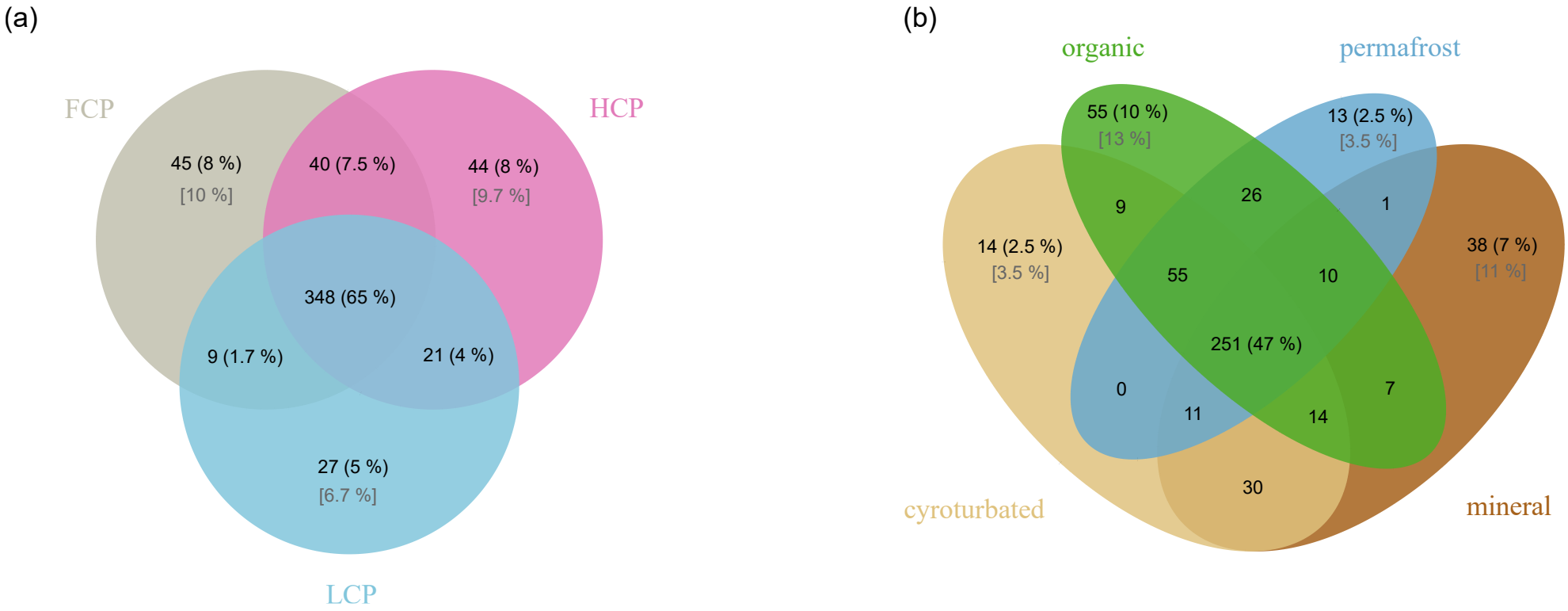

Supplementary Figure 2.: *Venn Diagrams depicting the number of shared and unique pyrolysis products among investigated (a) ice-wedge polygon types (n_LCP=20, n_FPT=32, n_HCP=29), and (b) soil layer categories (n_organic=35; n_mineral=14; n_cryoturbated=13, n_permafrost=19). Fractions of the shared and unique pyrolysis products from the total number of substances (n=534) are given in (%). Relative proportion of polygon-specific/soil layer-specific pyrolysis products relative to the total pyrolysis products per polygon type/ soil layer (grey) are given in [%].*

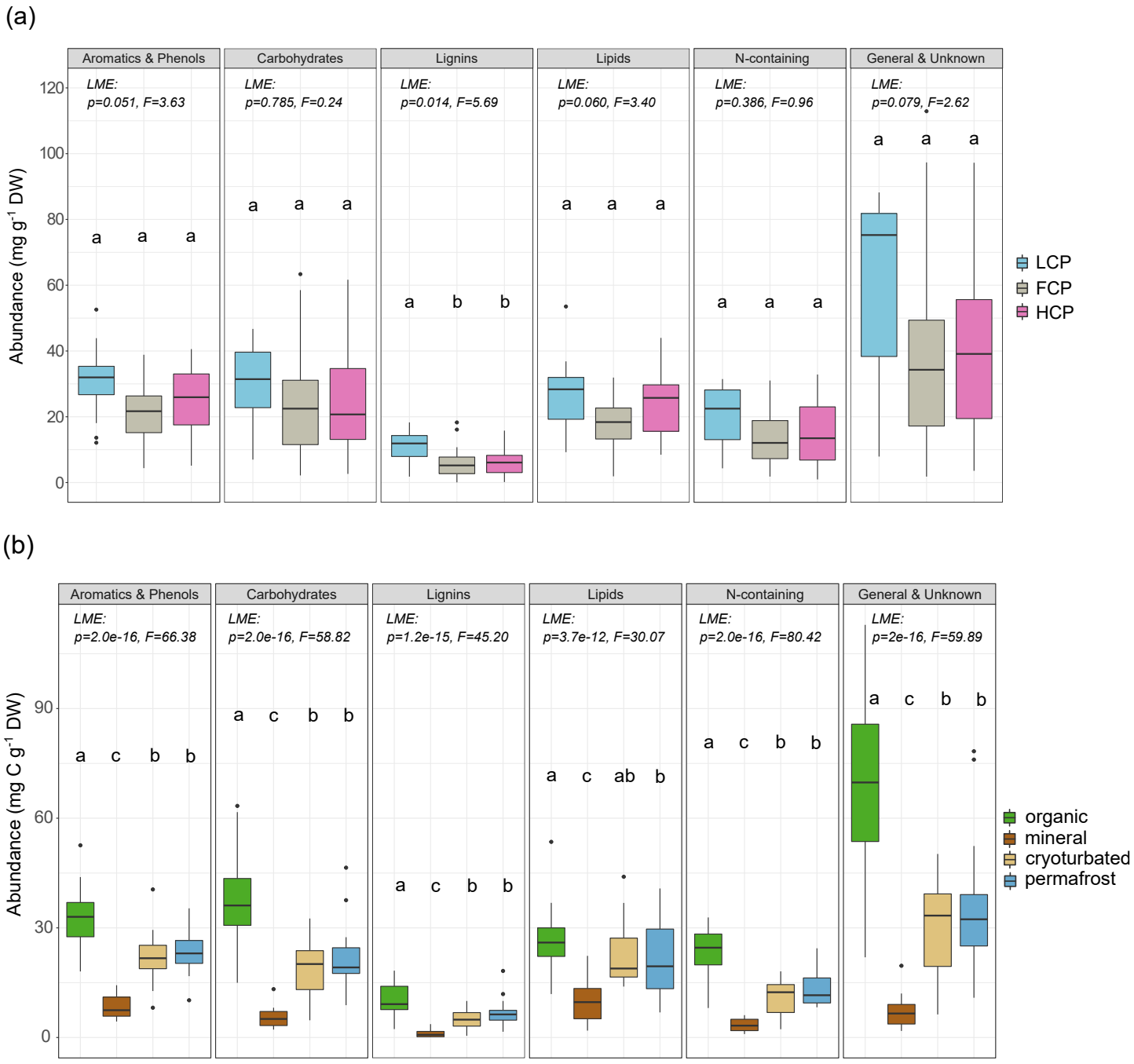

Supplementary Figure 3.: *Absolute abundances (mg g^{-1} DW) of SOM compound groups in investigated ice-wedge polygon types (n_LCP=20, n_FPT=32, n_HCP=29) and (b) soil layer categories (n_organic=35; n_mineral=14; n_cryoturbated=13, n_permafrost=19). Statistical results from linear mixed-effects models (Type II ANOVA p-values and F-statistics) are shown in respective panels. Pairwise comparisons (Tukey-adjusted emmeans) are indicated by letter groupings. No interactive effects between polygon type and soil layer category were observed.*

96

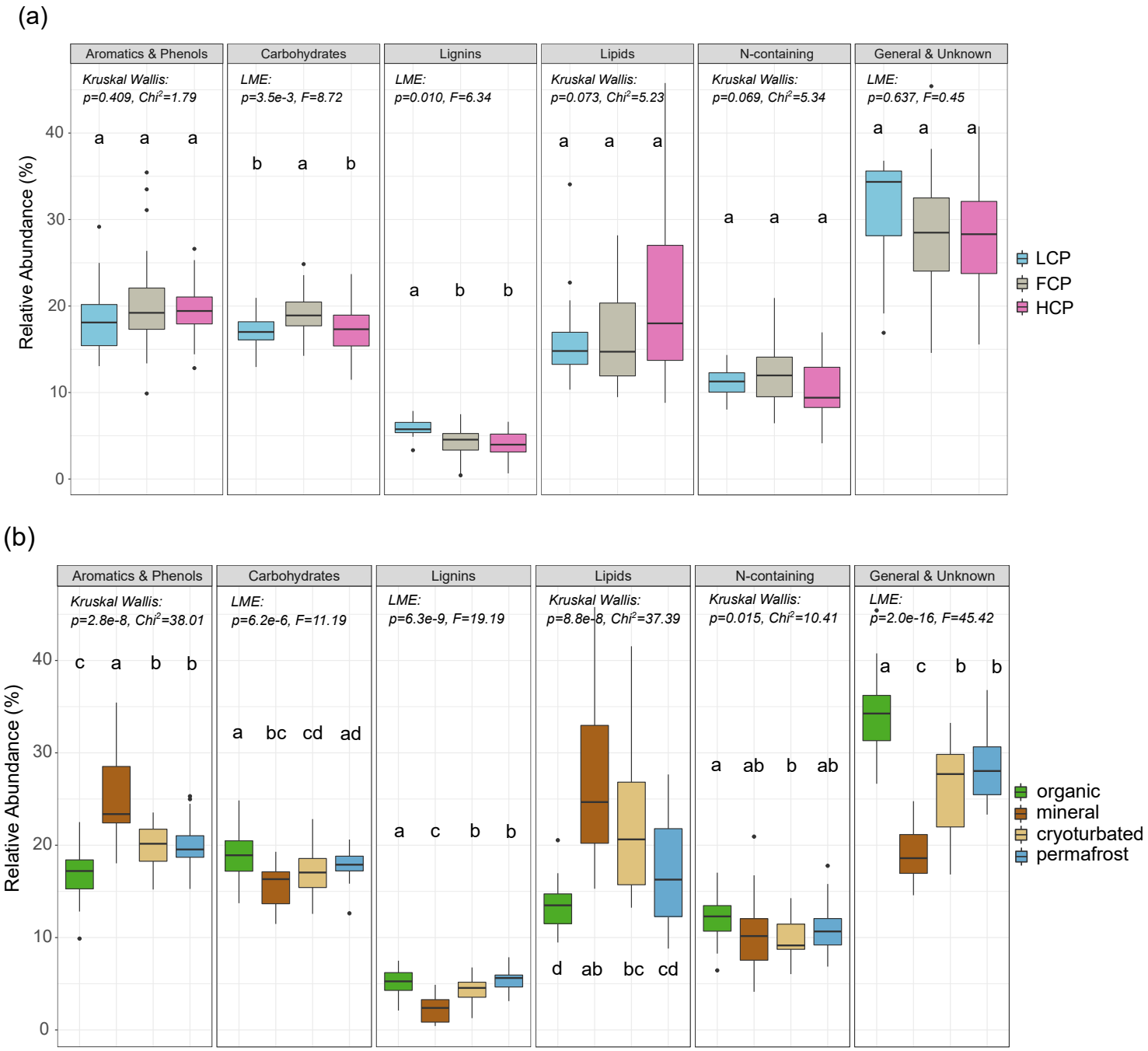

Supplementary Figure 4.: *Relative abundances (%) of SOM compound groups in investigated ice-wedge polygon types (n_LCP=20, n_FPT=32, n_HCP=29) and (b) soil layer categories (n_organic=35; n_mineral=14; n_cryoturbated=13, n_permafrost=19). Statistical results from linear mixed-effects models (Type II ANOVA p-values and F-statistics) are shown in respective panels. When model assumptions were not met, Kruskal–Wallis tests were used (p-values and Chi² statistics). Pairwise comparisons (Tukey-adjusted emmeans or Bonferroni-adjusted pairwise Wilcoxon tests) are indicated by letter groupings in brackets. No interactive effects between polygon type and soil layer category were observed.*

Section 4: Soil microbial communities

Microbial DNA was extracted using the FastDNA™ SPIN Kit for Soil (MP Biomedicals, Santa Ana, USA) following to the manufacturers' instructions but minor modifications for cleaning the samples from the RNAlater™ Stabilization Solution. We therefore added 1 ml sodium phosphate buffer (contained in the kit) and vortexed gently. After a short centrifugation step, we discarded the supernatant without disturbing the soil pellet and repeated the procedure five consecutive times. We followed the conventional DNA extraction protocol subsequently. Due to the large differences in bulk density, soil C and the assumed discrepancy in microbial biomass between the organic layer and the other layers, we used 250 mg FW soil from the organic topsoil and 400 mg FW soil from all other soil layers respectively. To control for potential contamination, extraction blanks were included and subjected to subsequent quantification and sequencing steps. DNA extracts were treated with the OneStep PCR Inhibitor Removal Kit (Zymo Research, Irvine, CA, USA) to remove possibly occurring inhibitory polyphenolics, humic- and fulvic acids, and tannins. DNA concentrations were quantified using the Quant-iT ™ PicoGreen® dsDNA Assay Kit (Thermo Fisher Scientific, Waltham, USA).

Amplicon sequencing and raw data processing was performed at the Joint Microbiome Facility of the Medical University of Vienna and the University of Vienna (JMF project ID JMF-2008-5). Datasets are deposited in the NCBI Sequence Read Archive under BioProject accession number (PRJNA1274918). We used DNA extracts that have been normalized to a concentration of 0.5 ng μl^{-1}. A two-step barcoding approach was employed to generate amplicon libraries of archaeal, bacterial, and fungal communities using Illumina MiSeq (V3 Kit) in the 2 x 300 bp configuration (Pjevac et al., 2021). The V4 hypervariable region of the 16S rRNA gene was amplified using primer pairs 515F (GTGYCAGCMGCCGCGGTAA, Parada et al., 2016) and 806R (GGACTACNVGGGTWTCTAAT, Apprill et al., 2015). The fungal ITS1 region was amplified using primer pairs ITS1F (CTTGGTCATTTAGAGGAAGTAA, Smith and Peay, 2014) and ITS2 (GCTGCGTTCTTCATCGATGC, White et al., 1990). First-step 25 µl PCR reactions consisted of 1x DreamTaq Green PCR master mix, 0.1 µg μl^{-1} BSA, 0.25 µmol l^{-1} of each headed primer, and 2 µl of DNA template. We used the following amplification conditions:

- 16S rRNA gene: initial denaturation at 94 °C for 3 min, followed by 30 cycles of 94 °C for 45 s, 52 °C for 60 s and 72 °C for 60 s, and final elongation at 72 °C for 10 min.
- ITS1 region: 94 °C for 1 min, 35 cycles of 94 °C for 45 s, 52 °C for 60 s and 72 °C for 90 s, followed by final elongation at 72 °C for 10 min.

Digital droplet PCR (ddPCR) was performed to quantify 16S rRNA genes and ITS1 regions with the same primers used for sequencing. Each ddPCR reaction had a volume of 22 µL and consisted of 1x QX200 ddPCR EvaGreen Supermix (BioRad), 0.1 µmol L^{-1} of each primer and 0.5 ng of template for the quantification of 16S rRNA genes or ITS1 regions, respectively. Droplets were generated on a QX200 ™ Droplet Generator (BioRad) and immediately subjected to PCR amplification (amplification conditions in Supplementary Table 5). PCR products in droplets were kept at 4 °C over night to increase their separation before measuring their fluorescence intensity on a QX200 ™ Droplet Reader (BioRad). Gene copy numbers were calculated using the QX ONE Software Standard Edition (v. 1.2, BioRad) where thresholds between positive and negative droplet populations were set consistently for each sample using the histogram as a guide. We expressed final ddPCR results as 16S rRNA and ITS1 gene copy numbers g^{-1} DW soil and used them as abundance proxies for bacteria and archaea, and fungi, respectively.

Prior downstream analyses, we cleaned the amplicon sequencing datasets from non-archaeal, -bacterial, or -fungal sequences and excluded samples with less than 500 obtained reads. Further, we corrected for possible contaminations during DNA extraction by subtracting the highest ASV-specific read number observed in the DNA extraction blanks from the corresponding ASV read number in the samples.

The resulting unfiltered count-datasets of bacterial and archaeal, and fungal reads were used to assess alpha-diversity after rarefication (we used the rarefy_even_depth()-function implemented in phyloseq, with the determined cut-offs at 2650 16S rRNA reads and at 543 ITS1 reads, respectively). We assessed alpha-diversity as richness (number of observed ASVs) and Shannon diversity.

We calculated abundances of individual ASVs (gene copy number corrected reads g^{-1} soil DW) by multiplying the 16S rRNA or ITS gene copy numbers measured in ddPCR assays with their respective relative abundances from the amplicon sequencing datasets. We discarded rare (bacterial, archaeal, and fungal) ASVs, defined as containing less than 0.05 % of all gene copy number corrected reads per sample. This resulted in 3643 bacterial and 137 archaeal ASVs (classified into 47 phyla, 111 classes, 201 orders, 247 families, and 308 genera) and 1604 fungal ASVs (classified into 7 phyla, 19 classes, 44 orders, 77 families and 101 genera) being considered in final analyses. For investigating the microbial community composition (β-diversity), we performed Principal Component Analyses (PCA) on center-log-ratio (clr) – transformed bacterial and archaeal, or fungal gene copy number corrected reads g^{-1} DW (Aitchinson distance). We used ddPCR-derived abundance data (gene copy number corrected reads g^{-1} DW) to explore quantitative differences of certain phyla between polygon types and soil layer categories.

167 ***Supplementary Table 5.:*** *ddPCR cycling conditions*

Temperature	***Time***	***Cycles***	***Details***	***Comments***
16S rRNA ddPCR quantification conditions				
95 °C	5 min			add a temperature ramp of 2 °C/second to all steps
95 °C	30 s	x 5	-1 °C every cycle	
57 °C	120 s			
95 °C	30 s	x 35		
52 °C	120 s			
4 °C	5 min			
90 °C	5 min			
4 °C	hold			
ITS1 Region ddPCR quantification conditions				
95 °C	5 min			add a temperature ramp of 2°C/second to all steps
95 °C	30 s	x 5	-1 °C every cycle	
60 °C	120 s			
95 °C	30 s	x 35		
55 °C	120 s			
4 °C	5 min			
90 °C	5 min			
4 °C	hold			

Supplementary Table 6(a).: *Microbial richness, diversity, and abundance among investigated ice-wedge polygon types.*

Bacteria & Archaea	**LCP**	**FCP**	**HCP**	**Polygon Type Effect**
Richness (No. ASVs)	494 ± 35 (b)	585 ± 33 (a) [n=30]	566 ± 38 (a)	**p = 0.013** (F = 6.1)
Diversity (Shannon Index)	4.95 ± 0.16 (b)	5.41 ± 0.1 (a) [n=30]	5.26 ± 0.13 (a)	**p = 2.2 e^{-3}** (F = 10.9)
Abundance (16S rRNA Gene Copies g^{-1} DW)	1.51e^{9} ± 4.24e^{8} (*int)	2.61e^{9} ± 4.42e^{8} (*int)	2.44e^{9} ± 4.48e^{8} (*int)	p = 0.116 (Chi² = 4.3)
Abundance (16S rRNA Gene copies mg^{-1} soil C)	4.21e^{6} ± 8.79e^{5} (b)	1.20e^{7} ± 1.40e^{6} (a)	9.98e^{6} ± 1.28e^{6} (a)	**p = 1.6 e^{-4}** (F = 16.6)
Fungi				
Richness (No. ASVs)	30 ± 3 (b) [n=19]	43 ± 4 (a) [n=30]	44 ± 4 (a)	**p = 5.9 e^{-3}** (F = 7.0)
Diversity (Shannon Index)	1.75 ± 0.19 (b) [n=19]	2.28 ± 0.15 (a) [n=30]	2.16 ± 0.16 (ab)	**p = 0.054** (F = 3.5)
Abundance (ITS1 Gene Region Copies g^{-1} DW)	1.05e^{7} ± 4.02e^{6} (*int)	7.26e^{7} ± 2.84e^{7} (*int)	1.08e^{8} ± 4.78e^{7} (*int)	p = 0.196 (Chi² = 3.3)
Abundance (ITS1 Gene Region Copies mg^{-1} soil C)	2.67e^{4} ± 8.88e^{3} (b)	2.03e^{5} ± 6.39e^{4} (a)	1.90e^{5} ± 5.70e^{4} (a) [n=28]	**p = 0.019** (Chi² = 8.0)

*Presented are means ± standard error (n_LCP=20, n_FPT=32, n_HCP=29; individual deviations noted in the table). Statistical results from linear mixed-effects models (Type II ANOVA p-values and F-statistics) are shown in the right column. When model assumptions were not met, Kruskal Wallis tests were used (p-values and Chi² statistics). Pairwise comparisons (Tukey-adjusted emmeans or Bonferroni-adjusted pairwise Wilcoxon tests) are indicated by letter groupings in brackets. Significant interactions between polygon type and soil layer are marked with (*int).*

Interactive effects:

Bacterial and archaeal abundance (16S rRNA gene copies g^{-1} DW) *was significantly lower in the organic layer of LCPs compared to FCPs and HCPs (Kruskal Wallis: p = 0.019, Chi^2 = 7.92; pairwise Wilcoxon: LCP vs. FCP p = 0.079, LCP vs. HCP p = 0.032). In the permafrost layer, bacterial and archaeal abundance was also significantly lower in LCPs than FCPs (Kruskal Wallis test: p = 0.011, Chi^2 = 8.94; pairwise Wilcoxon: LCP vs. FCP p = 0.010).*

Fungal abundance (ITS1 gene region copies g^{-1} DW) *was significantly lower in the organic layer of LCPs compared to FCPs and HCPs (Kruskal Wallis: p =3.51 e^{-4}, Chi^2 = 15.91; pairwise Wilcoxon: LCP vs. FCP p = 0.013, LCP vs. HCP p = p=4.6 e^{-4}).*

Supplementary Table 6(b).: *Microbial richness, diversity, and abundance among investigated soil layer categories.*

Bacteria & Archaea	**organic**	**mineral**	**cryoturbated**	**permafrost**	**Soil Layer Effect**
Richness (No. ASV)	702 ± 26 (a)	527 ± 37 (b)	452 ± 20 (bc) [n=11]	367 ± 16 (c)	**$p < 2e^{-16}$** ($F = 54.4$)
Diversity (Shannon Index)	5.72 ± 0.07 (a)	5.22 ± 0.13 (b)	4.91 ± 0.08 (bc) [n=11]	4.55 ± 0.12 (c)	**$p < 5.9e^{-16}$** ($F = 50.8$)
Abundance (16S rRNA Gene Copies g^{-1} DW)	$3.94e^{9} \pm 4.44e^{8}$ (*int)	$4.77e^{8} \pm 8.95e^{7}$ (*int)	$1.66e^{9} \pm 2.93e^{8}$ (*int)	$9.67e^{8} \pm 1.91e^{8}$ (*int)	**$p = 6.8e^{-8}$** ($Chi^2 = 36.2$)
Abundance (16S rRNA Gene copies mg^{-1} soil C)	$1.18e^{7} \pm 1.50e^{6}$ (a)	$7.96e^{6} \pm 1.26e^{6}$ (ab)	$9.20e^{6} \pm 1.40e^{6}$ (ab)	$5.91e^{6} \pm 1.33e^{6}$ (b)	**$p = 2.6e^{-3}$** ($F = 5.3$)
Fungi					
Richness (No. ASV)	52 ± 3 (a)	32 ± 5 (b)	39 ± 5 (b) [n=12]	24 ± 3 (b) [n=17]	**$p = 2.5e^{-7}$** ($F = 14.8$)
Diversity (Shannon Index)	2.43 ± 0.11 (a)	1.81 ± 0.22 (b)	2.19 ± 0.28 (ab) [n=12]	1.62 ± 0.22 (b) [n=17]	**$p = 1.1e^{-3}$** ($F = 6.1$)
Abundance (ITS1 Gene Region Copies g^{-1} DW)	$1.56e^{8} \pm 2.41e^{7}$ (*int)	$2.36e^{6} \pm 8.67e^{5}$ (*int)	$1.03e^{7} \pm 4.18e^{6}$ (*int) [n=13]	$2.46e^{6} \pm 1.11e^{6}$ (*int)	**$p = 3.9e^{-9}$** ($Chi^2 = 42.1$)
Abundance (ITS1 Gene Region Copies mg soil C^{-1})	$3.20e^{5} \pm 6.82e^{4}$ (a) [n=34]	$4.04e^{4} \pm 1.50e^{4}$ (*int)	$5.15e^{4} \pm 2.05e^{4}$ (*int) [n=13]	$1.33e^{4} \pm 5.61e^{3}$ (b)	**$p = 4.0e^{-7}$**($Chi^2 = 32.6$)

*Presented are means ± standard error (n_organic=35; n_mineral=14; n_cryoturbated=13, n_permafrost=19; individual deviations noted in the table). Statistical results from linear mixed-effects models (Type II ANOVA p-values and F-statistics) are shown in the right column. When model assumptions were not met, Kruskal Wallis tests were used (p-values and Chi² statistics). Pairwise comparisons (Tukey-adjusted emmeans or Bonferroni-adjusted pairwise Wilcoxon tests) are indicated by letter groupings in brackets. Significant interactions between polygon type and soil layer are marked with (*int).*

Interactive effects:

Bacterial and archaeal abundance (16S rRNA gene copies g^{-1} DW) *varied significantly among soil layers in all polygon types (Kruskal Wallis test: LCP p = 0.015, Chi² = 8.42; FCP p = 1.4 e^{-3}, Chi² = 15.59; HCP p = 3.9 e^{-5}, Chi² = 23.07). In each polygon type, the organic layer harbored higher bacterial and archaeal abundances than the permafrost layer (pairwise Wilcoxon tests: LCP p = 0.039; FCP p = 0.060; HCP p = 6.5 e^{-3}). in FCPs and HCPs, the organic layer additionally showed significantly higher abundances than the mineral layer (organic vs. mineral: FCP p = 0.026; HCP p = 6.5 e^{-3}).*

Fungal abundance (ITS1 gene region copies g^{-1} DW) *differed significantly among soil layers across all polygon types (Kruskal Wallis test: LCP p = 0.017, Chi² = 8.21; FCP p = 2.54 e^{-4}, Chi² = 19.15; HCP p = 6.88 e^{-5}, Chi² = 21.89). In each polygon type, the organic layer harbored higher fungal abundance than the permafrost layer (pairwise Wilcoxon tests: LCP p = 0.039; FCP p = 9.2 e^{-3}; HCP p = 6.5 e^{-3}). In FCPs and HCPs, fungal abundance in the organic layer was also higher than in both the mineral and cryoturbated layers (organic vs. mineral: FCP p = 0.005; HCP p = 6.5 e^{-3}; organic vs. cryoturbated: FCP p = 0.009; HCP p = 0.013).*

Fungal abundance normalized to soil carbon content (ITS1 gene copies mg-1 soil C) *varied significantly among soil layers within all polygon types (Kruskal Wallis test: LCP p = 0.026, Chi² = 7.30; FCP p = 9.4 e^{-4}, Chi² = 16.47; HCP p = 8.8 e^{-5}, Chi² = 21.4).In every polygon type, the organic layer showed higher fungal abundance per soil C than the permafrost layer (pairwise Wilcoxon tests: LCP p = 0.039; FCP p = 0.021; HCP p = 0.008). In FCPs and HCPs, fungal abundance in the organic layer also exceeded that in both the mineral and cryoturbated layers (organic vs. mineral: FCP p = 0.026, HCP p = 0.017; organic vs. cryoturbated: FCP p = 0.012, HCP p = 0.034). In HCPs, the permafrost layer had the lowest fungal abundance per soil C of all layers, with significantly lower values compared to both mineral (p = 0.030) and cryoturbated layers (p = 0.049).*

Supplementary Table 7.: *Interactive effects of polygon type and soil layer category on bacterial and archaeal community composition (corresponding to Fig. 3. in main text) P-values adjusted after Bonferroni; only significant results shown.*

Comparison	Result	Test
organic layer across all polygon types	p=0.001, F=4.33	Permanova
LCP vs. FCP	p=0.003, F=5.29	Pairwise adonis
LCP vs. HCP	p=0.003, F=7.16	
mineral layer across all polygon types	p=0.067, F=1.64	Permanova
cryoturbated layer across all polygon types	p=0.114, F=1.54	Permanova
permafrost layer across all polygon types	p=0.008, F=1.57	Permanova
LCP vs. FCP	p=0.003, F=2.09	Pairwise adonis
soil layers within LCPs	p=0.003, F=2.24	Permanova
organic vs. permafrost	p=0.006, F=3.37	Pairwise adonis
soil layers within FCPs	p=0.001, F=2.65	Permanova
organic vs. cryoturbated	p=0.006, F=2.80	Pairwise adonis
organic vs. permafrost	p=0.006, F=4.59	
soil layers within HCPs	p=0.001, F=3.80	Permanova
organic vs. mineral	p=0.006, F=3.94	Pairwise adonis
organic vs. cryoturbated	p=0.006, F=4.06	
organic vs. permafrost	p=0.006, F=5.71	
mineral vs. permafrost	p=0.024, F=3.13	
cryoturbated vs. permafrost	p=0.018, F=2.66	

171 ***Supplementary Table 8.:*** *Abundances (ddPCR-corrected reads g^{-1} DW soil) of selected bacterial and archaeal phyla in examined soil layers per polygon type.*

	Soil Layer	LCP	FCP	HCP	Polygon effect	Soil layer effect	Interactive effect
Acidobacteriota	organic	2.54 e^8 ± 1.07 e^8	7.27 e^8 ± 1.34 e^8	7.64 e^8 ± 1.37 e^8		Kruskal Wallis: p=4.1 e^{-9} Pairwise Wilcox: org-min: p=7.4 e^{-5} org-cryo: p=4.1 e^{-3} org-perm: 1.1 e^{-6}	Pairwise Wilcox organic: LCP-FCP: p=0.036 LCP-HCP: p=0.009 FCP-HCP: p=1.0
	mineral	9.36 e^6 ± 4.87 e^6	4.11 e^7 ± 9.96 e^6	4.69 e^7 ± 1.60 e^7			
	cryoturbated	-	5.74 e^7 ± 2.82 e^7	1.07 e^8 ± 4.04 e^7			
	permafrost	6.53 e^6 ± 3.09 e^6	4.42 e^7 ± 2.09 e^7	2.02 e^7 ± 1.11 e^7			
Actinobacteriota	organic	7.62 e^7 ± 2.43 e^7	1.44 e^8 ± 3.31 e^7	1.29 e^8 ± 2.10 e^7	LME: p=0.004 Emmeans pairwise: LCP-FCP: p=0.023 LCP-HCP: p=0.013 FCP-HCP: p=0.935	LME: p=3.7 e^{-6} Emmeans pairwise: org-min: p=0.023 org-cryo: p=0.961 org-perm: p=0.030	
	mineral	1.57 e^7 ± 7.14 e^6	2.18 e^7 ± 9.05 e^6	3.16 e^7 ± 7.95 e^6			
	cryoturbated	-	1.02 e^8 ± 1.65 e^7	1.76 e^8 ± 2.39 e^7			
	permafrost	2.06 e^7 ± 8.05 e^6	1.15 e^8 ± 4.32 e^7	6.45 e^7 ± 2.77 e^7			
Armatimonadota	organic	2.86 e^5 ± 1.80 e^5	3.19 e^6 ± 1.04 e^6	5.12 e^6 ± 1.97 e^6	Kruskal Wallis: p=9.5 e^{-3} Pairwise Wilcox: LCP-FCP: p=0.008 LCP-HCP: p=0.097 FCP-HCP: p=0.990		
	mineral	3.07 e^5 ± 3.07 e^5	1.37 e^6 ± 4.41 e^5	3.76 e^5 ± 9.97 e^4			
	cryoturbated	-	1.63 e^6 ± 1.01 e^6	4.99 e^5 ± 2.34 e^5			
	permafrost	4.65 e^5 ± 2.47 e^5	2.97e^6 ± 1.59 e^6	7.53 e^5 ± 4.86 e^5			
Bacteroidota	organic	5.83 e^8 ± 1.31 e^8	1.06 e^9 ± 2.36 e^8	1.02 e^9 ± 1.89 e^8		Kruskal-Wallis: p=1.6 e^{-6} Pairwise Wilcox: org-min: p=4.0 e^{-5} org-cryo: p=0.429 org-perm: 0.008	
	mineral	7.06 e^7 ± 4.17 e^7	1.09 e^8 ± 4.93 e^7	1.15 e^8 ± 4.54 e^7			
	cryoturbated	-	6.94 e^8 ± 2.20 e^8	3.36 e^8 ± 5.58 e^7			
	permafrost	1.21 e^8 ± 2.25 e^7	6.26 e^8 ± 1.46 e^8	2.68 e^8 ± 7.56 e^7			
Bdellovibrionota	organic	1.83 e^6 ± 1.13 e^6	5.44 e^6 ± 1.48 e^6	4.79 e^6 ± 2.05 e^6	Kruskal Wallis: p=5.7 e^{-4} Pairwise Wilcox: LCP-FCP: p=3.9 e^{-4}		
	mineral	2.01 e^5 ± 4.39 e^4	1.51 e^6 ± 1.16 e^6	1.61 e^6 ± 6.75 e^5			
	cryoturbated	-	8.90 e^6 ± 2.78 e^6	7.45 e^6 ± 2.19 e^6			

	permafrost	2.75 e^4 ± 2.75 e^4	3.22 e^6 ± 8.21 e^5	1.15 e^6 ± 8.83 e^5	LCP-HCP: p=0.016 FCP-HCP: p=0.904		
Caldisericota	organic	3.69 e^5 ± 2.45 e^5	0.00 ± 0.00	0.00 ± 0.00		The permafrost layer harbored 81 % of ddPCR-corr. reads assigned to this phylum.	
	mineral	8.93 e^5 ± 2.10 e^5	2.58 e^5 ± 2.58 e^5	0.00 ± 0.00			
	cryoturbated	-	3.69 e^5 ± 2.26 e^5	0.00 ± 0.00			
	permafrost	1.25 e^6 ± 4.43 e^5	1.85 e^6 ± 1.04 e6	3.37 e^6 ± 1.91 e^6			
Campylobacterota	organic	0.00 ± 0.00	0.00 ± 0.00	0.00 ± 0.00		The permafrost layer harbored 93 % of ddPCR-corr. reads assigned to this phylum.	
	mineral	0.00 ± 0.00	0.00 ± 0.00	0.00 ± 0.00			
	cryoturbated	-	2.48 e^5 ± 2.48 e^5	0.00 ± 0.00			
	permafrost	3.83 e^5 ± 2.86 e^5	9.41 e^5 ± 4.78 e^5	1.20 e^6 ± 1.11 e^6			
Cloacimonadota	organic	5.06 e^5 ± 3.29 e^5	0.00 ± 0.00	0.00 ± 0.00		The permafrost layer harbored 68 % of ddPCR-corr. reads assigned to this phylum.	
	mineral	0.00 ± 0.00	3.02 e^4 ± 3.02 e^4	0.00 ± 0.00			
	cryoturbated	-	0.00 ± 0.00	0.00 ± 0.00			
	permafrost	9.01 e^5 ± 7.55 e^5	9.28 e^5 ± 7.28 e^5	2.08 e^5 ± 1.25 e^5			
Cyanobacteria	organic	6.00 e^5 ± 3.68 e^5	1.73 e^6 ± 1.03 e^6	4.98 e^6 ± 1.70 e^6	LME: p=5.2 e Emmeans pairwise: LCP-FCP: p=0.318 LCP-HCP: p=0.013 FCP-HCP: p=0.120		
	mineral	1.54 e^5 ± 9.11 e^4	2.46 e^5 ± 1.79 e^5	7.25 e^5 ± 3.85 e^5			
	cryoturbated	-	1.01 e^6 ± 5.02 e^5	3.06 e^6 ± 1.40 e^6			
	permafrost	0.00 ± 0.00	1.81 e^5 ± 1.81 e^5	0.00 ± 0.00			
Crenarchaeota	organic	9.69 e^6 ± 3.64 e^6	2.60 e^6 ± 2.04 e^6	0.00 ± 0.00	Kruskal Wallis: p=2.3 e^{-5} Pairwise Wilcox: LCP-FCP: p=0.014 LCP-HCP: p=2.4 e^{-5} FCP-HCP: p=0.131		Pairwise Wilcox - organic: LCP-FCP: p=0.049 LCP-HCP: p=6.4 e^{-4} FCP-HCP: p=0.278
	mineral	2.63 e^4 ± 2.63 e^4	3.36 e^5 ± 2.00 e^5	6.23 e^4 ± 6.23 e^4			
	cryoturbated	-	9.07 e^4 ± 9.07 e^4	0.00 ± 0.00			
	permafrost	2.57 e^5 ± 1.45 e^5	9.62 e^4 ± 6.21 e^4	6.33 e^4 ± 4.06 e^4			
	organic	2.04 e^8 ± 5.97 e^7	7.89 e^7 ± 3.32 e^7	3.27 e^7 ± 1.25 e^7			

Desulfobacterota	mineral	1.66 e^7 ± 8.41 e^6	4.26 e^7 ± 2.04 e^7	1.27 e^7 ± 2.44 e^6			Pairwise Wilcox - organic: LCP-FCP: p=0.207 LCP- HCP: p=0.018 FCP-HCP: p=1.0
	cryoturbated	-	8.31 e^7 ± 2.23 e^7	2.31 e^7 ± 7.15 e^6			
	permafrost	1.41 e^7 ± 3.55 e^6	6.10 e^7 ± 1.16 e^7	2.05 e^7 ± 4.44 e^6			
Euryarchaeota	organic	8.11 e^7 ± 3.29 e^7	9.61 e^6 ± 6.85 e^6	3.00 e^5 ± 3.00 e^5	Kruskal Wallis: p=1.4 e^{-4} Pairwise Wilcox: LCP-FCP: p=0.005 LCP-HCP: p=1.9 e^{-4} FCP-HCP: p=0.972		Pairwise Wilcox organic: LCP-FCP: p=0.006 LCP-HCP: p=2.3 e^{-4} FCP-HCP: p=0.853
	mineral	3.52 e5 ± 1.59 e^4	5.00 e^5 ± 2.66 e^5	1.17 e^6 ± 5.67 e^5			
	cryoturbated	-	1.11 e^6 ± 5.09 e^5	1.29 e^6 ± 8.22 e^5			
	permafrost	1.34 e^6 ± 4.72 e^5	3.29 e^6 ± 1.46 e^6	1.67 e^6 ± 1.27 e^6			
Firmicutes	organic	1.24 e^7 ± 2.45 e^6	6.97 e^6 ± 2.34 e^6	5.53 e^6 ± 1.43 e^6		Kruskal Wallis: p=5.1 e^{-5} Pairwise Wilcox: perm-org: p=9.0 e^{-4} perm-min: p=3.4 e^{-4} perm-cryo: p=0.067	
	mineral	4.91 e^6 ± 3.30 e^6	5.40 e^6 ± 2.42 e^6	1.70 e^6 ± 8.04 e^5			
	cryoturbated	-	1.67 e^7 ± 7.69 e^6	5.08 e^6 ± 1.40 e^6			
	permafrost	2.30 e^7 ± 5.37 e^6	3.69 e^7 ± 1.25 e^7	2.34 e^7 ± 6.21 e^6			
Gemmatimonadota	organic	4.74 e^4 ± 4.74 e^4	1.23 e^7 ± 3.55 e^6	2.96 e^7 ± 6.59 e^6	Kruskal Wallis: p=3.0 e^{-8} Pairwise Wilcox: LCP-FCP: p=1.4 e^{-7} LCP-HCP: p=5.5 e^{-7} FCP-HCP: p=1.0		Pairwise Wilcox permafrost: LCP-FCP: p=0.02 LCP-HCP: p=0.22 FCP-HCP: p=0.25
	mineral	4.73 e^4 ± 4.73 e^4	3.96 e^6 ± 1.14 e^6	8.22 e^6 ± 3.78 e^6			
	cryoturbated	-	3.41 e^7 ± 2.3 e^7	1.93 e^7 ± 4.71 e^6			
	permafrost	0.00 ± 0.00	1.39 e^7 ± 9.38 e^6	1.63 e^6 ± 9.88 e^5			
Halobacterota	organic	1.36 e^7 ± 2.57 e^6	9.75 e^5 ± 7.23 e^5	1.42 e^5 ± 1.42 e^5	Kruskal Wallis: p=3.6 e^{-5} Pairwise Wilcox: LCP-FCP: p=2.1 e^{-4} LCP-HCP: p=2.0 e^{-4} FCP-HCP: p=1.0		Pairwise Wilcox organic: LCP-FCP: p=1.6 e^{-4} LCP-HCP: p=1.0 e^{-4} FCP-HCP: p=1.0
	mineral	4.00 e^6 ± 1.52 e^6	1.89 e^6 ± 1.51 e^6	1.84 e^6 ± 1.42 e^6			
	cryoturbated	-	5.29 e^6 ± 2.72 e^6	4.40 e^6 ± 1.18 e^6			
	permafrost	4.22 e^6 ± 1.86 e^6	4.03 e^6 ± 1.80 e^6	5.09 e^6 ± 1.37 e^6			
Latescibacterota	organic	8.54 e^6 ± 3.95 e^6	0.00 ± 0.00	1.22 e^6 ± 9.36 e^5			LCP organic harbored 88 % of ddPCR-corr. reads
	mineral	3.07 e^5 ± 3.07 e^5	5.50 e^4 ± 3.81 e^4	0.00 ± 0.00			
	cryoturbated	-	0.00 ± 0.00	0.00 ± 0.00			

	permafrost	1.10 e^4 ± 1.10 e^4	0.00 ± 0.00	0.00 ± 0.00			assigned to this phylum
Methylomirabilota	organic	4.04 e^6 ± 8.17 e^5	2.12 e^6 ± 1.71 e^6	3.24 e^5 ± 3.24 e^5		The permafrost layer harbored < 1 % of ddPCR-corr. reads assigned to this phylum.	LCP organic harbored 60 % of ddPCR-corr. reads assigned to this phylum
	mineral	2.10 e^5 ± 1.58 e^5	2.13 e^5 ± 1.54 e^5	1.24 e^5 ± 8.18 e^4			
	cryoturbated	-	0.00 ± 0.00	0.00 ± 0.00			
	permafrost	1.18 e^5 ± 7.52 e^4	0.00 ± 0.00	0.00 ± 0.00			
Micrarchaeota	organic	2.57 e^6 ± 9.44 e^5	1.17 e^6 ± 1.17 e^6	0.00 ± 0.00			LCP organic harbored 69 % of ddPCR-corr. reads assigned to this phylum
	mineral	0.00 ± 0.00	0.00 ± 0.00	0.00 ± 0.00			
	cryoturbated	-	0.00 ± 0.00	0.00 ± 0.00			
	permafrost	0.00 ± 0.00	0.00 ± 0.00	0.00 ± 0.00			
Myxococcota	organic	9.63 e^6 ± 6.20 e^6	2.71 e^7 ± 7.93 e^6	3.59 e^7 ± 5.74 e^6			Pairwise Wilcox organic: LCP-FCP: p=0.104 LCP-HCP: p=0.007 FCP-HCP: p=0.765
	mineral	1.91 e^5 ± 5.44 e^4	1.25 e^5 ± 1.11 e^5	1.58 e^6 ± 6.00 e^5			
	cryoturbated	-	1.68 e^6 ± 8.45 e^5	2.83 e^6 ± 7.48 e^5			
	permafrost	0.00 ± 0.00	6.73 e^5 ± 6.73 e^5	0.00 ± 0.00			
Nanoarchaeota	organic	4.56 e^7 ± 1.47 e^7	3.03 e^7 ± 1.34 e^7	6.63 e^5 ± 4.58 e^5			LCP organic harbored 48 % of ddPCR-corr. reads assigned to this phylum.
	mineral	1.93 e^6 ± 1.87 e^6	1.83 e^6 ± 1.09 e^6	5.80 e^5 ± 3.89 e^5			
	cryoturbated	-	1.87 e^7 ± 8.03 e^6	8.24 e^5 ± 6.60 e^5			
	permafrost	1.85 e^6 ± 7.68 e^5	1.26 e^7 ± 8.25 e^6	4.87 e^5 ± 2.10 e^5			
Patescibacteria	organic	4.81 e^7 ± 1.00 e^7	2.55 e^7 ± 9.85 e^6	1.15 e^7 ± 3.84 e^6			Emmeans pairwise organic: LCP-FCP: p=0.211 LCP-HCP: p=0.009 FCP-HCP: p=0.320
	mineral	4.46 e^6 ± 6.95 e^5	1.52 e^7 ± 8.10 e^6	1.71 e^7 ± 1.03 e^7			
	cryoturbated	-	7.14 e^7 ± 2.35 e^7	4.54 e^7 ± 1.22 e^7			
	permafrost	1.17 e^7 ± 5.39 e^6	5.00 e^7 ± 1.01 e^7	1.52 e^7 ± 3.66 e^6			
	organic	1.53 e^7 ± 5.40 e^6	5.21 e^7 ± 1.69 e^7	5.15 e^7 ± 8.91 e^6			

Planctomycetota	mineral	0.00 ± 0.00	1.49 e^{6} ± 5.60 e^{5}	2.47 e^{6} ± 1.21 e^{6}		.	Pairwise Wilcox - organic: LCP-FCP: p=0.235 LCP-HCP: p=0.005 FCP-HCP: p=1.0
	cryoturbated	-	4.92 e^{6} ± 2.93 e^{6}	4.63 e^{6} ± 1.92 e^{6}			
	permafrost	1.32 e^{5} ± 1.07 e^{5}	1.65 e^{6} ± 8.07 e^{5}	1.06 e^{6} ± 9.46 e^{5}			
Proteobacteria	organic	2.45 e^{8} ± 7.11 e^{7}	7.06 e^{8} ± 1.40 e^{8}	8.26 e^{8} ± 1.77 e^{8}	Kruskal Wallis: p=0.008 Pairwise Wilcox: LCP-FCP: p=0.05 LCP-HCP: p=0.008 FCP-HCP: p=1.0	Kruskal Wallis: p=2.9 e^{-5} Pairwise Wilcox: org-min: p=1.6 e^{-4} org-cryo: p=1.0 org-perm: p=0.015	
	mineral	7.07 e^{6} ± 2.06 e^{5}	6.16 e^{7} ± 2.44 e^{7}	1.42 e^{8} ± 3.47 e^{7}			
	cryoturbated	-	4.89 e^{8} ± 3.21 e^{8}	4.29 e^{8} ± 9.87 e^{7}			
	permafrost	9.90 e^{7} ± 4.57 e^{7}	3.27 e^{8} ± 9.45 e^{7}	2.18 e^{8} ± 9.26 e^{7}			
RCP2-54	organic	3.19 e^{5} ± 3.19 e^{5}	7.00 e^{6} ± 2.40 e^{6}	2.23 e^{6} ± 7.31 e^{5}	LCPs harbored 2.5 % of ddPCR-corr. reads assigned to this phylum.		
	mineral	0.00 ± 0.00	7.81 e^{5} ± 4.02 e^{5}	2.61 e^{6} ± 1.61 e^{6}			
	cryoturbated	-	8.30 e^{5} ± 7.02 e^{5}	2.13 e^{6} ± 1.40 e^{6}			
	permafrost	0.00 ± 0.00	0.00 ± 0.00	4.32 e^{5} ± 3.82 e^{5}			
Sva0485	organic	6.91 e^{6} ± 2.49 e^{6}	0.00 ± 0.00	0.00 ± 0.00			LCP organic harbored 99.6 % of ddPCR-corr. reads assigned to this phylum
	mineral	1.84 e^{5} ± 1.84 e^{5}	0.00 ± 0.00	0.00 ± 0.00			
	cryoturbated	-	0.00 ± 0.00	0.00 ± 0.00			
	permafrost	0.00 ± 0.00	0.00 ± 0.00	0.00 ± 0.00			
TA06	organic	1.81 e^{6} ± 5.15 e^{5}	0.00 ± 0.00	0.00 ± 0.00			LCP organic harbored 97 % of ddPCR-corr. reads assigned to this phylum
	mineral	3.68 e^{5} ± 3.68 e^{5}	0.00 ± 0.00	0.00 ± 0.00			
	cryoturbated	-	0.00 ± 0.00	0.00 ± 0.00			
	permafrost	0.00 ± 0.00	0.00 ± 0.00	0.00 ± 0.00			
Unknown Taxa on Phylum level	organic	7.58 e^{6} ± 5.74 e^{6}	1.45 e^{6} ± 7.18 e^{5}	4.23 e^{5} ± 4.23 e^{5}		The permafrost layer harbored 43 % of ddPCR-corr. reads assigned to this phylum.	
	mineral	2.55 e^{6} ± 1.99 e^{6}	1.89 e^{6} ± 1.02 e^{6}	1.09 e^{6} ± 4.20 e^{5}			
	cryoturbated	-	1.18 e^{7} ± 3.97 e^{6}	2.03 e^{6} ± 7.93 e^{5}			

	permafrost	4.17 e^6 ± 1.40 e^6	1.46 e^7 ± 5.94 e^6	4.90 e^6 ± 2.12 e^6			
Verrucomicrobiota	organic	1.61 e^8 ± 4.78 e^7	8.19 e^8 ± 1.35 e^8	8.99 e^8 ± 1.15 e^8	Kruskal Wallis: p=0.0150 Pairwise Wilcox: LCP-FCP: p=0.035 LCP-HCP: p=0.027 FCP-HCP: p=1.0	Kruskal Wallis: p=1.08 e^{-8} Pairwise Wilcox: org-min: p=9.1 e^{-5} org-cryo:p=0.087 org-perm: p=3.1 e^{-6}	
	mineral	2.94 e^7 ± 5.19 e^6	4.11 e^7 ± 1.07 e^7	7.80e^7 ± 2.48 e^7			
	cryoturbated	-	2.35 e^8 ± 1.54 e^8	1.91 e^8 ± 3.53 e^7			
	permafrost	1.14 e^7 ± 5.77 e^6	1.04 e^8 ± 4.74 e^7	2.45 e^7 ± 1.10 e^7			
WPS-2	organic	5.56 e^5 ± 4.10 e^5	3.67 e^6 ± 1.80 e^6	4.04 e^6 ± 2.36 e^6	LCPs harbored 6.4 % of ddPCR-corr. reads assigned to this phylum.		
	mineral	0.00 ± 0.00	4.11 e^5 ± 2.52 e^5	0.00 ± 0.00			
	cryoturbated	-	5.41 e^5 ± 5.41 e^5	5.84 e^5 ± 3.89 e^5			
	permafrost	0.00 ± 0.00	0.00 ± 0.00	0.00 ± 0.00			

Presented are means ± standard error (LCP_organic: n=12, FCP_organic: n=12, HCP_organic: n=11, LCP_mineral: n=2, FCP_mineral: n=6, HCP_mineral: n=6, FCP_cryoturbated: n=5, HCP_cryoturbated: n=6, LCP_permafrost: n=6, FCP_permafrost: n=7, HCP_permafrost: n=6). Effects of polygon type, soil layer category, and their interaction were tested either using LME (ANOVA type III) or Kruskal Wallis test, followed by pairwise comparisons (Tukey-adjusted emmeans pairwise tests and Bonferroni-adjusted pairwise Wilcoxon tests). For space saving reasons, the presented statistics refer to the observations discussed in the main text. If phylum abundances were too imbalanced for statistical testing, other relevant abundance information is stated instead.

172 ***Supplementary Table 9.:*** *Abundances (ddPCR-corrected reads g^{-1} DW soil) of fungal phyla in examined soil layers per polygon type.*

	Soil layer	LCP	FCP	HCP	Polygon effect	Soil layer effect	Interactive effect
Ascomycota	organic	$1.04\ e^{7} \pm 3.18\ e^{6}$	$6.61\ e^{7} \pm 2.18\ e^{7}$	$8.70\ e^{7} \pm 2.44\ e^{7}$	Kruskal Wallis: p=0.361	Kruskal Wallis: p=9.3 e^{-9} The organic layer harbored 96.7 % of ddPCR-corr. reads assigned to this phylum.	LCP organic harbored 6.4 % of ddPCR-corr. reads assigned to this phylum.
	mineral	$3.45\ e^{5} \pm 3.11\ e^{5}$	$7.37\ e^{5} \pm 4.23\ e^{5}$	$1.63\ e^{6} \pm 1.08\ e^{6}$			
	cryoturbated	-	$7.81\ e^{5} \pm 3.61\ e^{5}$	$2.56\ e^{6} \pm 5.03\ e^{5}$			
	permafrost	$6.18\ e^{5} \pm 3.10\ e^{5}$	$4.07\ e^{6} \pm 2.03\ e^{6}$	$3.34\ e^{5} \pm 2.16\ e^{5}$			
Basidiomycota	organic	$3.32\ e^{5} \pm 2.77\ e^{5}$	$2.00\ e^{7} \pm 6.36\ e^{6}$	$3.16\ e^{7} \pm 1.46\ e^{7}$	Kruskal Wallis: p=0.023 Pairwise Wilcox: LCP-FCP: p=0.049 LCP-HCP: p=0.055 FCP-HCP: p=1.0	Kruskal Wallis: p=3.6 e^{-6} The organic layer harbored 99 % of ddPCR-corr. reads assigned to this phylum.	LCP organic harbored < 1% of ddPCR-corr. reads assigned to this phylum.
	mineral	$1.02\ e^{3} \pm 1.02\ e^{3}$	$8.50\ e^{4} \pm 5.86\ e^{4}$	$2.54\ e^{5} \pm 2.39\ e^{5}$			
	cryoturbated	-	$3.68\ e^{4} \pm 2.64\ e^{4}$	$4.78\ e^{5} \pm 4.60\ e^{5}$			
	permafrost	$5.86\ e^{3} \pm 4.65\ e^{3}$	$2.23\ e^{4} \pm 1.02$ e4	$1.33\ e^{4} \pm 1.21\ e^{4}$			
Chytridiomycota	organic	$3.97\ e^{3} \pm 3.33\ e^{3}$	$1.35\ e^{6} \pm 7.79\ e^{5}$	$5.27\ e^{6} \pm 3.16\ e^{6}$	Kruskal Wallis: p=0.047 Pairwise Wilcox: LCP-FCP: p=0.047 LCP-HCP: p=0.087 FCP-HCP: p=1.0	Kruskal Wallis: p=2.9 e^{-4} The organic layer harbored > 99 % of ddPCR-corr. reads assigned to this phylum.	LCP organic harbored < 1% of ddPCR-corr. reads assigned to this phylum.
	mineral	0.00 ± 0.00	$7.18\ e^{2} \pm 4.80\ e^{2}$	$8.11\ e^{2} \pm 7.07\ e^{2}$			
	cryoturbated	-	$2.18\ e^{3} \pm 1.68\ e^{3}$	$2.16\ e^{4} \pm 2.16\ e^{4}$			
	permafrost	0.00 ± 0.00	0.00 ± 0.00	0.00 ± 0.00			
Kickxellomycota	organic	$1.15\ e^{4} \pm 1.10\ e^{4}$	$3.06\ e^{5} \pm 2.53\ e^{5}$	$7.06\ e^{3} \pm 7.06\ e^{3}$	Kruskal Wallis: p=0.898	The organic layer harbored 94 % of ddPCR-corr. reads assigned to this phylum.	LCP organic harbored < 5% of ddPCR-corr. reads assigned to this phylum.
	mineral	0.00 ± 0.00	0.00 ± 0.00	0.00 ± 0.00			
	cryoturbated	-	$6.77\ e^{3} \pm 6.77\ e^{3}$	3.37 e^{3} ± 3.37 e3			
	permafrost	0.00 ± 0.00	0.00 ± 0.00	$2.51\ e^{3} \pm 2.51\ e^{3}$			
Mortierellomycota	organic	0.00 ± 0.00	$4.25\ e^{4} \pm 4.25\ e^{4}$	9.03 e^{4} ± 5.51 e4	Phylum is absent from LCP soils	The organic layer harbored 82 % of ddPCR-corr. reads	
	mineral	0.00 ± 0.00	$2.73\ e^{3} \pm 2.73\ e^{3}$	$3.67\ e^{2} \pm 2.40\ e^{2}$			
	cryoturbated	-	$3.14\ e^{3} \pm 2.18\ e^{3}$	$4.14\ e^{4} \pm 4.14\ e^{4}$			

	permafrost	0.00 ± 0.00	4.58 e^3 ± 2.09 e^3	2.13 e^3 ± 2.13 e^3		assigned to this phylum.	
Rozellomycota	organic	0.00 ± 0.00	1.48 e^5 ± 1.03 e^5	2.30 e^3 ± 2.12 e^6	Phylum is absent from LCP soils.	The organic layer harbored 82 % of ddPCR-corr. reads assigned to this phylum.	LCP organic harbored >1 % of ddPCR-corr. reads assigned to this phylum.
	mineral	0.00 ± 0.00	0.00 ± 0.00	0.00 ± 0.00			
	cryoturbated	-	2.01 e^2 ± 2.01 e^2	0.00 ± 0.00			
	permafrost	0.00 ± 0.00	0.00 ± 0.00	0.00 ± 0.00			
Unknown Taxa on phylum level	organic	6.11 e^6 ± 3.39 e6	9.61 e^7 ± 4.33 e^7	4.62 e^7 ± 1.39 e^7	Kruskal-Wallis: p=0.083	Kruskal Wallis: p=0.025 The organic layer harbored > 92 % of ddPCR-corr. reads unassigned at phylum level	
	mineral	3.75 e4 ± 4.58 e3	1.31 e^6 ± 6.52 e^5	1.34 e^6 ± 6.85 e^5			
	cryoturbated	-	6.52 e^6 ± 4.24 e^6	1.23 e^7 ± 7.57 e^6			
	permafrost	5.49 e^5 ± 5.25 e^5	2.12 e^6 ± 1.08 e^6	2.30 e^5 ± 1.13 e^5			
Zoopagomycota	organic	0.00 ± 0.00	0.00 ± 0.00	5.66 e^4 ± 5.66 e^4	Phylum is solely present in HCP organic.	Phylum is solely present in HCP organic.	HCP organic harbored 100% of ddPCR-corr. reads assigned to this phylum.
	mineral	0.00 ± 0.00	0.00 ± 0.00	0.00 ± 0.00			
	cryoturbated	-	0.00 ± 0.00	0.00 ± 0.00			
	permafrost	0.00 ± 0.00	0.00 ± 0.00	0.00 ± 0.00			

Presented are means ± standard error (LCP_organic: n=12, FCP_organic: n=12, HCP_organic: n=11, LCP_mineral: n=2, FCP_mineral: n=6, HCP_mineral: n=6, FCP_cryoturbated: n=6, $HCP_{cryoturbated}$: n=6, LCP_permafrost: n=5, FCP_permafrost: n=6, HCP_permafrost: n=6, except for Basidiomycota: HCP_organic: n=10). Effects of polygon type, soil layer category, and their interaction were tested either using LME (ANOVA type III) or Kruskal Wallis test, followed by pairwise comparisons (Tukey-adjusted emmeans pairwise tests and Bonferroni-adjusted pairwise Wilcoxon tests). For space saving reasons, the presented statistics refer to the observations discussed in the main text. If phylum abundances were too imbalanced for statistical testing, other relevant abundance information is stated instead.

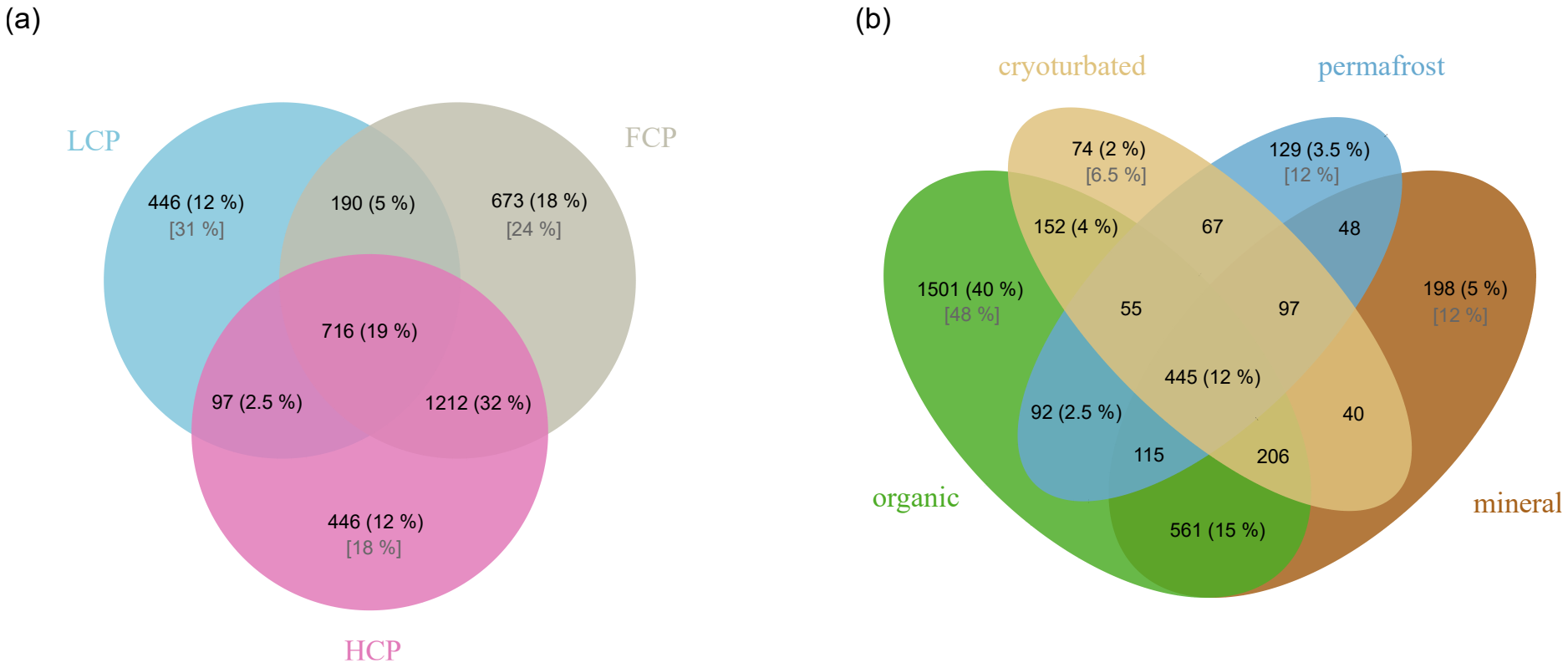

Supplementary Figure 5.: *Venn Diagram depicting the number of shared and unique bacterial and archaeal ASVs among investigated* ***(a)*** *ice-wedge polygon types (n_LCP=19, n_FPT=30, n_HCP=29) and* ***(b)*** *soil layer categories (n_organic=35, n_mineral=14, n_cryoturbated=11, n_permafrost=19). Fractions of the shared and unique taxa from the total number of substances (n=3780) are given in (%). Relative proportion of polygon-specific/ soil layer-specific ASVs relative to total ASVs per polygon type/soil layer (grey) are given in [%].*

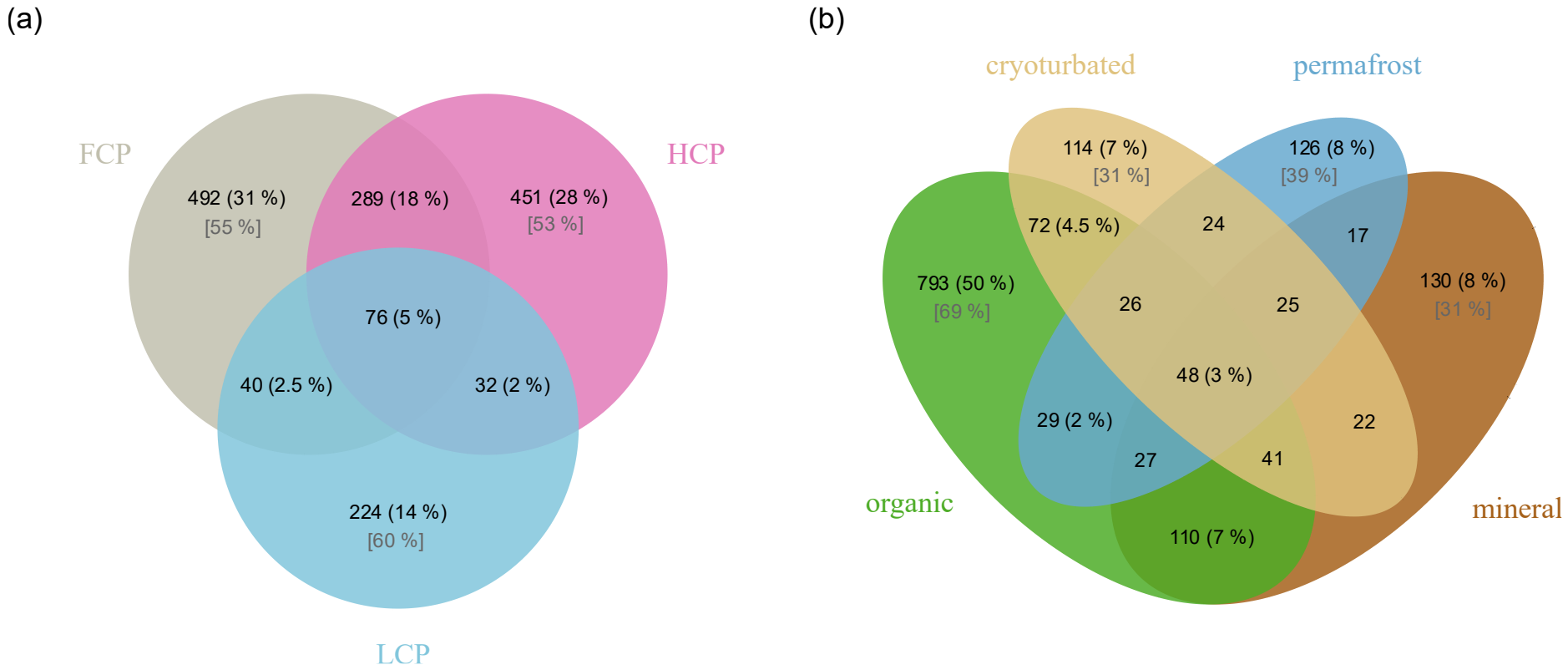

Supplementary Figure 6.: *Venn Diagram depicting the number of shared and unique fungal ASVs among investigated (a) ice-wedge polygon types (n_LCP=19, n_FPT=30, n_HCP=29) and (b) soil layer categories (n_organic=35, n_mineral=14, n_cryoturbated=12, n_permafrost=17). Fractions of the shared and unique taxa from the total number of substances (n=1604) are given in (%). Relative proportion of polygon-specific/ soil layer-specific ASVs relative to total ASVs per polygon type/soil layer (grey) are given in [%].*

Section 5: Extracellular enzymatic activity potential

We measured the potential activities of the six hydrolytic extracellular enzymes: β-D-1,4-cellobiosidase (exoglucanase), β-D-1,4-glucosidase, β-1,4-N-acetyl- glucosaminidase (exochitinase), leucine-aminopeptidase (protease), acid phosphatase, and sulfatase (Aryl-sulfate sulfohydrolase), using microplate fluorometric assays as described in Canarini et al., 2021. Per sample, one gram of soil was suspended in 100 ml sodium acetate buffer (100 mM, pH 5.5) and subsequently sonicated to an energy absorption of 350 J. 200 µl of the soil suspension and 50 µl of substrate were pipetted into black microtiter plates in five technical replicates. The used substrates were: 4-MUF-β-D-cellobioside, 4-MUF-β-D-glucoside, 4-MUF-N-acetyl-β-D-glucosaminide, L-Leucine-7-amino-4-methylcoumarin, 4-MUF-phosphate, 4-MUF-sulfate. 4-Methylumbelliferone (MUF) was used as standard for cellobiosidase, β-glucosidase, exochitinase, phosphatase and sulfatase, whereas 7-Amino-4-methylcoumarine (AMC) was used to calibrate protease activity. All plates were incubated at 20 °C for 15 minutes in the dark and fluorescence was measured at 365 nm excitation and 450 nm emission (Tecan Infinite M200fluorimeter, Werfen, Austria) every 30 minutes for 3 hours. Potential extracellular enzymatic activities were calculated considering the increase in fluorescence between measurement time points.

Supplementary Table 10.: *Correlation between enzyme activities (nmol g^{-1} DW h^{-1}) and Soil C, N, P contents (mg g^{-1} DW).*

	Soil C	Soil N	Soil P
Betaglucosidase	ρ (79) = 0.743; **$p < 2.2\ e^{-16}$**		
Exoglucanase	ρ (77) = 0.646 **$p < 2.2\ e^{-16}$**		
Exochitinase	ρ (78) = 0.471 **$p = 1.30\ e^{-5}$**	ρ (78) = 0.471 **$p = 1.32\ e^{-5}$**	
Leucine-Aminopeptidase	ρ (79) = 0.663 **$p < 2.2\ e^{-16}$**	ρ (79) = 0.660 **$p < 2.2\ e^{-16}$**	
Acid Phosphatase	ρ (79) = 0.810 **$p < 2.2\ e^{-16}$**		ρ (78) = 0.594 **$p = 1.18\ e^{-8}$**
Sulfatase	ρ (75) = 0.680 **$p < 2.2\ e^{-16}$**		

Presented are Spearman's Rank Order correlation coefficient rho (ρ(df)) and respective p-values (two-sided test)..

Supplementary Table 11: *Interactive effects of polygon type and soil layer category on extracellular enzymatic activity potentials (nmol substrate g^{-1} soil C h^{-1}; corresponding to Fig. 5. in main text).*

Soil Layer	Polygon	Betaglucosidase (emmeans)	Exoglucanase (pairwise Wilcox)	Exochitinase (emmeans)	Leucine Aminopeptidase (pairwise Wilcox)	Acid Phosphatase (pairwise Wilcox)
organic	LCP vs. FCP	p<0.0001	p=0.003	p=0.010	p=0.070	p=0.0007
	LCP vs. HCP	p=0.001	p=0.002		p=0.063	
	FCP vs. HCP	p=0.035		p=0.034		
mineral	LCP vs. FCP					
	LCP vs. HCP					
	FCP vs. HCP					
cryoturbated	FCP vs. HCP					
permafrost	LCP vs. FCP		p=0.010	p=0.026		
	LCP vs. HCP			p=0.006		
	FCP vs. HCP		p=0.025			

Polygon	Soil Layer	Betaglucosidase (emmeans)	Exoglucanase (pairwise Wilcox)	Exochitinase (emmeans)	Leucine Aminopeptidase (pairwise Wilcox)	Acid Phosphatase (pairwise Wilcox)
LCP	organic vs. mineral					
	organic vs. permafrost					
	mineral vs. permafrost					
FCP	organic vs. mineral	p<0.0001	p=0.043			p=0.010
	organic vs. cryoturbated	p<0.0001				p=0.028
	organic vs. permafrost	p=0.006			p=0.036	p=0.003
	mineral vs. cryoturbated					
	mineral vs. permafrost	p=0.012				
	cryoturbated vs. permafrost					
HCP	organic vs. mineral	p<0.0001	p=0.076			
	organic vs. cryoturbated	p=0.020	p=0.062	p=0.0001		
	organic vs. permafrost	p=0.006	p=0.034	p=0.003	p=0.013	
	mineral vs. cryoturbated			p=0.002		
	mineral vs. permafrost			p=0.030		
	cryoturbated vs. permafrost					

Only relevant results (significant or almost significant) for pairwise comparisons (Tukey-adjusted emmeans tests following LME, or Bonferroni-adjusted pairwise Wilcox test following Kruskal Wallis test) are shown. Note that no interaction occurred for sulfatase activity.

194

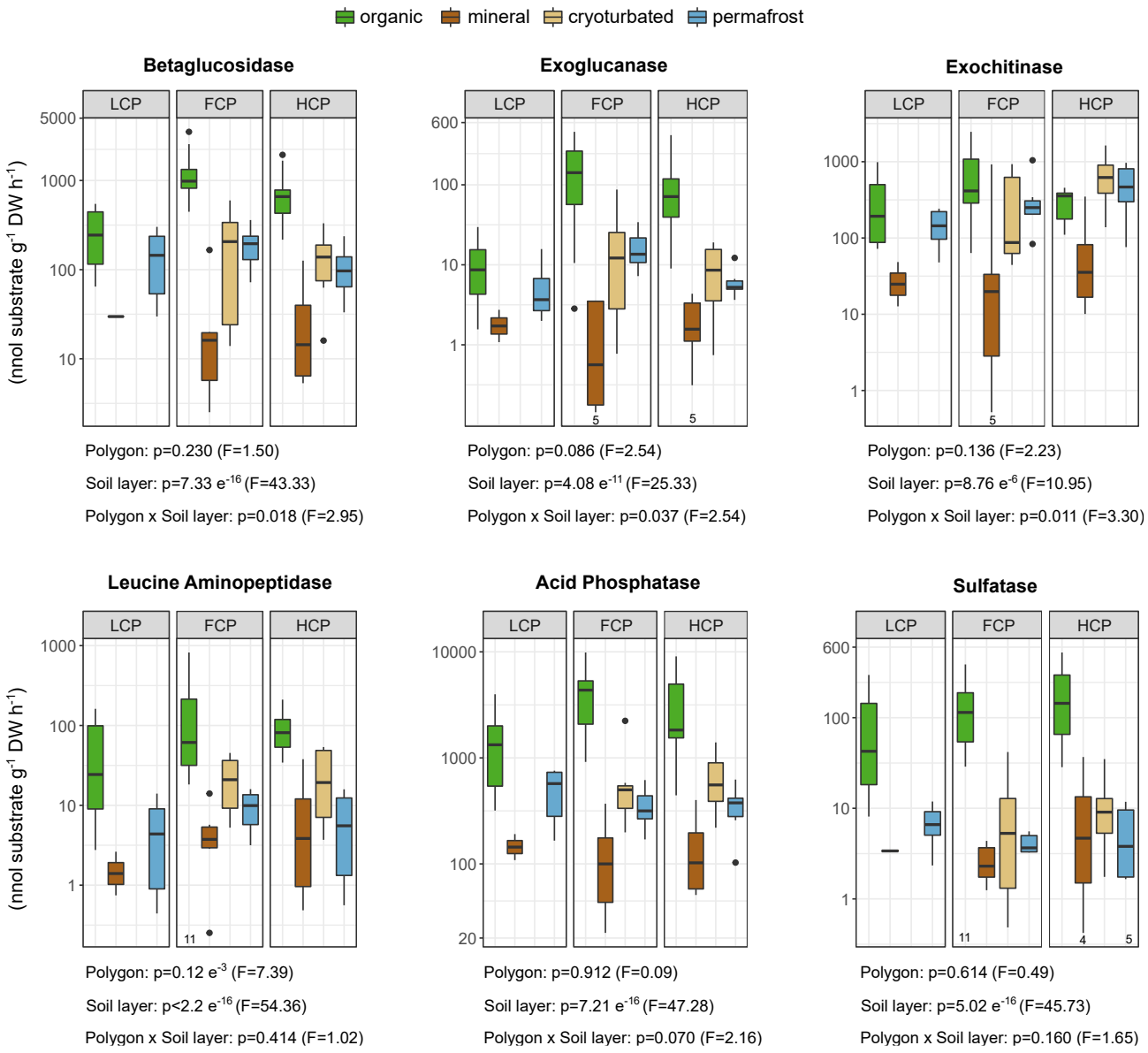

Supplementary Figure 7.:. *Extracellular enzymatic activity potential in investigated soil layer categories and ice-wedge polygon types. Rates (nmol substrate g^{-1} DW h^{-1}) are depicted on a log-scale for improved readability (LCP_organic: n=12, FCP_organic: n=12, HCP_organic: n=11, LCP_mineral: n=2, FCP_mineral: n=6, HCP_mineral: n=6, FCP_cryoturbated: n=7, HCP_cryoturbated: n=6, LCP_permafrost: n=6, FCP_permafrost: n=7, HCP_permafrost: n=6; with deviations stated below respective boxplots). Effects of polygon type and soil layer category are stated under respective panels (LME ANOVA type III test results). Please note that N-, P- and S-depolymerizing enzymes are inherently related to the C-cycle, which hinders the clear differentiation between microbial nutrient- versus C acquisition.*

Interactive effects:

Organic: *The organic layer of LCPs had lower betaglucosidase- (emmeans LCP vs. FCP: p<0.0001, t=-5.1, LCP vs. HCP: p=0.007, t=-3.2), exoglucanase- (emmeans: LCP vs. FCP: p<0.0001, t=-5.1, LCP vs. HCP: p=0.0004, t=-4.2), and acid phosphatase- (emmeans: LCP vs. FCP: p=0.002, t=-3.6, LCP vs. HCP: p=0.065, t=-2.3) -rates than the organic layers of FCPs and HCPs.*

***Permafrost**: The permafrost layer of LCPs had lower exochitinase rates than the permafrost samples of HCPs (emmeans: LCP vs. HCP: p=0.055, t=-2.4).*

Section 6: Statistics

We employed linear-mixed-effects models (lmes) to test all univariate variables for the fixed effects of 'ice-wedge polygon type' and 'soil layer category' plus their interaction. Therefore, we used the packages lme4 (Bates et al., 2015), lmerTest (Kuznetsova et al., 2017), emmeans,(Lenth et al., 2022) and car (Fox and Weisberg, 2019). While we acknowledge the difference in glaciation history between the examined sites, we anticipated only negligible historical influences on the characteristics of the recent SOM pool and microbial communities. Due to the sites' very similar landscape, climate, soils, and vegetation, we determined the random effect in the lme model as specific soil pit ID blocked within the sampling site (model<-lmer(variable~polygon.type*soil.layer.category + (1|site/soil pit)). Model results were inspected using the anova() function with the default being a type III analysis of variance (ANOVA). In the case of no interactive effect being observed we used type II ANOVA to account for potential effects of different treatment replicates (Langsrud, 2003) . We used the Estimated Marginal Means post hoc test to perform multiple comparisons on the fixed effects of polygon type and soil layer category (emmeans(model,pairwise~Polygon.type,adjust='tukey'), ememans(model,pairwise~Soil.layer.category,adjust='tukey'). In the case of an interactive effect being observed by ANOVA result and /or visual investigation of the data, we compared (a) differences between soil layers per type of polygon (emmeans(model,pairwise~Soil.layer.category|Polygon.type, adjust='tukey') and (b) differences between polygon types per soil layer category (emmeans(model,pairwise~ Polygon.type |Soil.layer.category, adjust='tukey'). We checked for homogeneity of variances and normality of model residuals by inspecting frequency histograms, boxplots, QQ-plots, and via Shapiro and Levene tests. If model assumptions were not met, a log- or sqrt-transformation was applied. In case of no agreement with model assumptions after transformation, we conducted nonparametric tests. Kruskal Wallis tests were used to test the effects of Polygon.type and Soil.layer.category, followed by pairwise two-sided Wilcoxon tests (function pairwise.wilcox.test(), p.adjust='bonferroni'). We also applied Wilcoxon tests on respectively subsetted parts of the dataset to check for possible interactive effects in a comparable manner as described for the lme models and additionally used faceted boxplots for checking the distribution of the examined parameter among all soil layer categories within each type of polygon.

We employed the phyloseq package (McMurdie and Holmes, 2013) for handling the multivariate datasets on amplicon sequencing and SOM chemical composition. Following Alteio et al., 2021, we applied a centered log-ratio (clr) data normalization (microbiome::

transform(phyloseq.object, “clr”) and calculated euclidean distance matrices (phyloseq::distance(phyloseq.object, "euclidean"). We performed Principal Component Analyses (PCAs) for visualization, employing the function ‘phyloseq::ordinate()’. We used Permutational Multivariate Analysis of Variance (PERMANOVA) to explore the effects of polygon type and soil layer category and their possible interaction (adonis()-function implemented in vegan with 999 permutations and p-adjust.m=’bonferroni’; vegan version 2.5-7, Oksanen at al., 2020). We tested differences between polygon types and/or soil layer categories by pairwise multilevel comparisons (paiwise.adonis()-function implemented in vegan with 999 permutations and p.adjust.m=’bonferroni)’. In case of interactive effects, we used subsetted datasets for making pairwise tests. Analogously as described for the lme model, we tested for (a) differences between soil layers within each polygon type and (b) for differences between polygon types for each soil layer. As PERMANOVA test results are sensitive to heterogenous dispersions among the investigated groups, we tested their variance of dispersion using Permutation Tests for Multivariate Dispersion Homogeneity (PERMDIST), implemented in vegan (vegan::betadisper()-function) using 999 permutations and the argument ‘bias.adjust=T’ for unequal sample numbers (Anderson, 2017). We used Venn diagrams (get_vennlist(phyloseq.object) for visualizing the fraction of shared versus unique pyrolysis products and/or microbial ASVs among polygon types and soil layers respectively (MicrobiotaProcess package, Xu et al., 2022)

Section 7: References:

Alteio, L. V., Séneca, J., Canarini, A., Angel, R., Jansa, J., Guseva, K., Kaiser, C., Richter, A., Schmidt, H., 2021. A critical perspective on interpreting amplicon sequencing data in soil ecological research. Soil Biol. Biochem. 160. https://doi.org/10.1016/j.soilbio.2021.108357

Anderson, M., 2017. Permutational Multivariate Analysis of Variance (PERMANOVA). pp. 1–15. https://doi.org/10.1002/9781118445112.stat07841

Apprill, A., McNally, S., Parsons, R., Weber, L., 2015. Minor revision to V4 region SSU rRNA 806R gene primer greatly increases detection of SAR11 bacterioplankton . Aquat. Microb. Ecol. 75, 129–137.

Bates, D., Mächler, M., Bolker, B., Walker, S., 2015. Fitting Linear Mixed-Effects Models Using lme4. J. Stat. Softw. 67, 1–48. https://doi.org/10.18637/jss.v067.i01

Beck, H., Zimmermann, N., McVicar, T., Vergopolan, N., Berg, A., Wood, E., 2018. Present and future Köppen-Geiger climate classification maps at 1-km resolution. Sci. Data 5, 180214. https://doi.org/10.1038/sdata.2018.214

Brooks, G.R., Lane, L.S., 2011. A guide to the landscape of the Firth River Valley, Ivvavik National Park [WWW Document]. Geol. Surv. Canada, Park. Canada, Nat. Resour. Canada. URL https://publications.gc.ca/collections/collection_2017/pc/R64-404-2011-eng.pdf

Buurman, P., Van Bergen, P.F., Jongmans, A.G., Meijer, E.L., Duran, B., Van Lagen, B., 2005. Spatial and temporal variation in podzol organic matter studied by pyrolysis-gas chromatography/mass spectrometry and micromorphology. Eur. J. Soil Sci. 56, 253–270. https://doi.org/https://doi.org/10.1111/j.1365-2389.2004.00662.x

Canarini, A., Schmidt, H., Fuchslueger, L., Martin, V., Herbold, C.W., Zezula, D., Gündler, P., Hasibeder, R., Jecmenica, M., Bahn, M., Richter, A., 2021. Ecological memory of recurrent drought modifies soil processes via changes in soil microbial community. Nat. Commun. 12, 1–14. https://doi.org/10.1038/s41467-021-25675-4

Couture, N.J., Pollard, W.H., 2017. A Model for Quantifying Ground-Ice Volume, Yukon Coast, Western Arctic Canada. Permafr. Periglac. Process. 28, 534–542. https://doi.org/https://doi.org/10.1002/ppp.1952

D'Angelo, E., Crutchfield, J., 2001. Rapid, Sensitive, Microscale Determination of Phosphate in Water and Soil. J. Environ. Qual. 30, 2206.

Dunnington D, 2023. gspatial: Spatial Data Framework for ggplot2.

Dyke, A., Prest, V., 1987. Late Wisconsinan and Holocene History of the Laurentide Ice Sheet. Géographie Phys. Quat. 41, 237–263. https://doi.org/https://doi.org/10.7202/032681ar

Esri, 2024. Esri World Imagery. "World Hillshade" [basemap] [WWW Document].

Fox, J., Weisberg, S., 2019. An R Companion to Applied Regression. Third Ed. Sage Thousand Oaks, CA, USA.

Frank-Fahle, B.A., Yergeau, É., Greer, C.W., Lantuit, H., Wagner, D., 2014. Microbial functional potential and community composition in permafrost-affected soils of the NW Canadian Arctic. PLoS One 9. https://doi.org/10.1371/journal.pone.0084761

Fritz, M., Wetterich, S., Schirrmeister, L., Meyer, H., Lantuit, H., Preusser, F., Pollard, W.H., 2012. Eastern Beringia and beyond: Late Wisconsinan and Holocene landscape dynamics along the Yukon Coastal Plain, Canada. Palaeogeogr. Palaeoclimatol. Palaeoecol. 319–320, 28–45. https://doi.org/10.1016/j.palaeo.2011.12.015

González-Pérez, M., Buurman, P., Vidal-Torrado, P., Martin-Neto, L., 2012. Pyrolysis-Gas Chromatography/Mass Spectrometry Characterization of Humic Acids in Coastal Spodosols from Southeastern Brazil. Soil Sci. Soc. Am. J. 76, 961–971. https://doi.org/https://doi.org/10.2136/sssaj2011.0178

Government of Canada, 2024. Canadian Climate Normals & Averages [WWW Document]. URL http://climate.weather.gc.ca/climate_normals/index_e.html

Hempfling, R., Schulten, H.R., 1990. Chemical characterization of the organic matter in forest soils by Curie point pyrolysis-GC/MS and pyrolysis-field ionization mass spectrometry. Org. Geochem. 15, 131–145. https://doi.org/10.1016/0146-6380(90)90078-E

Irwin, A., 2021. Data Visualization [WWW Document]. Mak. Maps. URL https://andrewirwin.github.io/data-visualization/mapping-1.html#further-reading-21

Kahle, D., Wickham, H., 2013. ggmap: Spatial Visualization with ggplot2. R J. 5, 144–161. https://doi.org/10.32614/RJ-2013-014

Kim, S., Chen, J., Cheng, T., Gindulyte, A., He, J., He, S., Li, Q., Shoemaker, B.A., Thiessen, P.A., Yu, B., Zaslavsky, L., Zhang, J., Bolton, E.E., 2023. PubChem 2023 update. Nucleic Acids Res. 51, D1373–D1380. https://doi.org/10.1093/nar/gkac956

Kuo, S., 1996. Phosphorus. In Methods of Soil Analysis, Part 3: Chemical Methods. Soil Science Society of America.

Kuznetsova, A., Brockhoff, P.B., Christensen, R.H.B., 2017. lmerTest Package: Tests in Linear Mixed Effects Models. J. Stat. Softw. 82, 1–26. https://doi.org/10.18637/jss.v082.i13

Langsrud, Ø., 2003. ANOVA for unbalanced data: Use Type II instead of Type III sums of squares. Stat. Comput. 13, 163–167.

Lenth, R. V, Buerkner, P., Herve, M., Love, J., Miguez, F., Riebl, H., Singmann, H., 2022. Package “Emmeans”(Version R Package 1.7. 2): Estimated Marginal Means, Aka Least-Squares Means [Computer Software].

Martin, V., Schmidt, H., Canarini, A., Koranda, M., Hausmann, B., Müller, C.W., Richter, A., 2024. Soil cover shapes organic matter pools and microbial communities in soils of maritime Antarctica. Geoderma 446, 116894. https://doi.org/https://doi.org/10.1016/j.geoderma.2024.116894

McMurdie, P.J., Holmes, S., 2013. phyloseq: An R Package for Reproducible Interactive Analysis and Graphics of Microbiome Census Data. PLoS One 8, 1–11. https://doi.org/10.1371/journal.pone.0061217

Ninnes, S., Tolu, J., Meyer-Jacob, C., Mighall, T.M., Bindler, R., 2017. Investigating molecular changes in organic matter composition in two Holocene lake-sediment records from central Sweden using pyrolysis-GC/MS. J. Geophys. Res. Biogeosciences 122, 1423–1438. https://doi.org/10.1002/2016JG003715

Parada, A.E., Needham, D.M., Fuhrman, J.A., 2016. Every base matters: assessing small subunit rRNA primers for marine microbiomes with mock communities, time series and

global field samples. Environ. Microbiol. 18, 1403–1414. https://doi.org/https://doi.org/10.1111/1462-2920.13023

Pebesma, E., 2018. Simple Features for R: Standardized Support for Spatial Vector Data. R J. 10, 439–446. https://doi.org/10.32614/RJ-2018-009

Pjevac, P., Hausmann, B., Schwarz, J., Kohl, G., Herbold, C.W., Loy, A., Berry, D., 2021. An Economical and Flexible Dual Barcoding, Two-Step PCR Approach for Highly Multiplexed Amplicon Sequencing. Front. Microbiol. 12. https://doi.org/10.3389/fmicb.2021.669776

Rampton, V.N., 1982. Quaternary Geology Yukon Coastal Plain, Yukon Territory-Northwest Territory [WWW Document]. https://doi.org/https://doi.org/10.4095/111348

Said, M., John, G., Mhilu, C., Manyele, S., 2015. The Study of Kinetic Properties and Analytical Pyrolysis of Coconut Shells. J. Renew. Energy 2015, 307329. https://doi.org/https://doi.org/10.1155/2015/307329

Saiz-Jimenez, C., De Leeuw, J.W., 1986. Chemical characterization of soil organic matter fractions by analytical pyrolysis-gas chromatography-mass spectrometry. J. Anal. Appl. Pyrolysis 9, 99–119. https://doi.org/10.1016/0165-2370(86)85002-1

Schulten, H.R., Schnitzer, M., 1997. The chemistry of soil organic nitrogen: A review. Biol. Fertil. Soils 26, 1–15. https://doi.org/10.1007/s003740050335

Shen, Q., Suarez-Abelenda, M., Camps-Arbestain, M., Calvelo Pereira, R., McNally, S.R., Kelliher, F., 2018. Data on the organic matter characteristics of New Zealand soils under different land uses. Data Br. 21, 620–638. https://doi.org/https://doi.org/10.1016/j.dib.2018.10.016

Smith, D.P., Peay, K.G., 2014. Sequence depth, not PCR replication, improves ecological inference from next generation DNA sequencing. PLoS One 9, e90234. https://doi.org/10.1371/journal.pone.0090234

Soil Classification Working Group, 1998. The Canadian System of Soil Classification, 3rd ed. Ag. ed.

Speetjens, N.J., Tanski, G., Martin, V., Wagner, J., Richter, A., Hugelius, G., Boucher, C., Lodi, R., Knoblauch, C., Koch, B.P., Wünsch, U., Lantuit, H., Vonk, J.E., 2022. Dissolved organic matter characterization in soils and streams in a small coastal low-Arctic catchment. Biogeosciences 19, 3073–3097. https://doi.org/10.5194/bg-19-3073-2022

Stewart, C.E., 2012. Evaluation of angiosperm and fern contributions to soil organic matter using two methods of pyrolysis-gas chromatography-mass spectrometry. Plant Soil 351, 31–46. https://doi.org/10.1007/s11104-011-0927-3

Tarnocai, C., 2004. Northern Soil Research in Canada - Cryosols: Permafrost-Affected Soils, in: Kimble, J.M. (Ed.), . Springer Berlin Heidelberg, Berlin, Heidelberg, pp. 29–43. https://doi.org/10.1007/978-3-662-06429-0_3

Tolu, J., Gerber, L., Boily, J.-F., Bindler, R., 2015. High-throughput characterization of sediment organic matter by pyrolysis–gas chromatography/mass spectrometry and multivariate curve resolution: A promising analytical tool in (paleo)limnology. Anal. Chim. Acta 880, 93–102. https://doi.org/https://doi.org/10.1016/j.aca.2015.03.043

Vancampenhout, K., Wouters, K., De Vos, B., Buurman, P., Swennen, R., Deckers, J., 2009. Differences in chemical composition of soil organic matter in natural ecosystems from

different climatic regions - A pyrolysis-GC/MS study. Soil Biol. Biochem. 41, 568–579. https://doi.org/10.1016/j.soilbio.2008.12.023

Wagner, J., Martin, V., Speetjens, N.J., A'Campo, W., Durstewitz, L., Lodi, R., Fritz, M., Tanski, G., Vonk, J.E., Richter, A., Bartsch, A., Lantuit, H., Hugelius, G., 2023. High resolution mapping shows differences in soil carbon and nitrogen stocks in areas of varying landscape history in Canadian lowland tundra. Geoderma 438, 116652. https://doi.org/10.1016/j.geoderma.2023.116652

Walker, D.A., Raynolds, M.K., Daniëls, F.J.A., Einarsson, E., Elvebakk, A., Gould, W.A., Katenin, A.E., Kholod, S.S., Markon, C.J., Melnikov, E.S., Moskalenko, N.G., Talbot, S.S., Yurtsev, B.A.(†., Team, T. other members of the C., 2005. The Circumpolar Arctic vegetation map. J. Veg. Sci. 16, 267–282. https://doi.org/https://doi.org/10.1111/j.1654-1103.2005.tb02365.x

Westerveld, L., Kurvits, T., Schoolmeester, T., Eckhoff, T., Overduin, P., Fritz, M., Alfthan, B., Sinisalo, A., Mulelid, O., 2023. Arctic Permafrost Atlas. https://doi.org/10.61523/KPJI4549

White, Bruns, T., Lee, S., Taylor, J., 1990. White, T. J., T. D. Bruns, S. B. Lee, and J. W. Taylor. Amplification and direct sequencing of fungal ribosomal RNA Genes for phylogenetics. pp. 315–322.

Wickham, H., 2016. ggplot2: Elegant Graphics for Data Analysis, Use R! Springer International Publishing.

Xu, S., Li, Z., Tang, W., Dai, Z., Zhou, L., Feng, T., Chen, M., Liu, S., Fu, X., Wu, T., Hu, E., Yu, G., 2022. MicrobiotaProcess: A comprehensive R package for managing and analyzing microbiome and other ecological data within the tidy framework. https://doi.org/10.21203/rs.3.rs-1284357/v1